NASA TECHNICAL NOTE

NASA TN D-6004

INVESTIGATION OF CHAR FORMATION AND SURFACE RECESSION OF A COMPOSITE ABLATION MATERIAL WITH A SILICONE-RESIN BASE

by Allen G. McLain

Langley Research Center
Hampton, Va. 23365

NATIONAL AERONAUTICS AND SPACE ADMINISTRATION • WASHINGTON, D. C. • OCTOBER 1970

1. Report No. NASA TN D-6004	2. Government Accession No.	3. Recipient's Catalog No.
4. Title and Subtitle INVESTIGATION OF CHAR FORMATION AND SURFACE RECESSION OF A COMPOSITE ABLATION MATERIAL WITH A SILICONE-RESIN BASE		5. Report Date October 1970 6. Performing Organization Code
7. Author(s) Allen G. McLain		8. Performing Organization Report No. L-6359
9. Performing Organization Name and Address NASA Langley Research Center Hampton, Va. 23365		10. Work Unit No. 124-07-18-06 11. Contract or Grant No.
12. Sponsoring Agency Name and Address National Aeronautics and Space Administration Washington, D.C. 20546		13. Type of Report and Period Covered Technical Note 14. Sponsoring Agency Code
15. Supplementary Notes		

16. Abstract

A composite ablation material containing a silicone-resin base, silica fibers, and phenolic and silica hollow microspheres has been subjected to a wide range of test conditions to study its charring behavior. The ablation tests were performed at stagnation-point pressures ranging from 0.016 to 1.3 atm and heating rates ranging from 1.34 MW/m^2 to 14.8 MW/m^2 in air and nitrogen. The resulting char-layer surfaces fell into three categories – black char, glassy-coated char, and gray char – as heating rates (and char surface temperatures) were increased. The char layers formed contained large percentages by weight of silicon dioxide. Silicon carbide was found to be in chars formed at high heating rates. Empirical correlations of surface recession were determined. For the higher heating rates where steady-state ablation was approached, char-layer constituents and mass loss could be predicted adequately with chemical equilibrium in the reactions at the surface assumed.

17. Key Words (Suggested by Author(s)) Ablation Silicone-resin-based material Surface chemistry Char differences Mechanical removal	18. Distribution Statement Unclassified – Unlimited		
19. Security Classif. (of this report) Unclassified	20. Security Classif. (of this page) Unclassified	21. No. of Pages 41	22. Price* $3.00

*For sale by the Clearinghouse for Federal Scientific and Technical Information
Springfield, Virginia 22151

INVESTIGATION OF CHAR FORMATION AND SURFACE RECESSION OF A COMPOSITE ABLATION MATERIAL WITH A SILICONE-RESIN BASE

By Allen G. McLain
Langley Research Center

SUMMARY

A composite ablation material containing a silicone-resin base, silica fibers, and phenolic and silica hollow microspheres has been subjected to a wide range of test conditions to study its charring behavior. The ablation tests were performed at stagnation-point pressures ranging from 0.016 to 1.3 atm and heating rates ranging from 1.34 MW/m^2 to 14.8 MW/m^2 in air and nitrogen. The resulting char-layer surfaces fell into three categories – black char, glassy-coated char, and gray char – as heating rates (and char surface temperatures) were increased. The char layers formed contained large percentages by weight of silicon dioxide. Silicon carbide was found to be in chars formed at high heating rates. Empirical correlations of surface recession were determined. For the higher heating rates where steady-state ablation was approached, char-layer constituents and mass loss could be predicted adequately with chemical equilibrium in the reactions at the surface assumed.

INTRODUCTION

One of the problem areas in the analytical study of the ablation of a charring heat-shield material is the representation of the chemical reactions occurring at the ablating surface. The problem is simplified by assuming that the reactions between the species of the boundary-layer gases, of the char, and of the pyrolysis gases are in chemical equilibrium. For materials containing carbon, oxygen, hydrogen, and nitrogen, this assumption has proven not only a simplification but an adequate method, in some cases of predicting the mass loss observed experimentally (ref. 1). For ablation materials containing silicon in addition to the four elements mentioned, the problem is complicated further by the fact that the char surface can be one of three condensed species: silicon dioxide, silicon carbide, or carbon, depending on temperature and pressure. In order for an equilibrium solution for such a material system to provide a good comparison with experimental results, the surface condensed species as well as mass-loss data must be accurately predicted.

A composite silicone-resin-based material, developed at the Langley Research Center and designated E4A1, was used in this study to determine the surface behavior of a material system containing the elements C, O, H, N, and Si. In this study, E4A1 was charred over a wide range of heating rates at several constant-pressure levels from 0.01 to 1.0 atm in both the Langley 20-inch hypersonic arc-heated tunnel (HAHT) and the high-enthalpy arc tunnel (HEAT) at the Langley Research Center. The resulting char layers were analyzed with powder X-ray diffraction techniques and by standard chemical means to determine the surface species. The identification of surface species along with measured surface recession and temperature provided a comparison with an equilibrium-surface-thermochemistry (EST) solution.

The results of this experimental investigation of the surface behavior of a silicone-resin-based material, along with the chemical-equilibrium comparisons, are presented in this paper.

SYMBOLS

B'	nondimensional mass loss, $\dot{m}/h$
c_p	heat capacity, J/kg-^{o}K
h	heat-transfer coefficient corrected for gaseous injection, kg/m^2-sec
h_o	heat-transfer coefficient uncorrected for gaseous injection, kg/m^2-sec
l	thickness, m
ΔL	model recession, mm
$\Delta L/\Delta t$	char recession-rate parameter, mm/sec
$\dot{m}$	mass-loss rate, kg/m^2-sec
p_s	stagnation-point pressure (1 atm = 101.3 kN/m^2)
$\dot{q}$	cold-wall heating rate, W/m^2
r	effective hemispherical nose radius, m

r_b	body radius, cm
r_c	corner radius, cm
r_n	nose radius, cm
s	distance from stagnation point along surface, figures 2 and 4, mm
T	surface temperature, ^{o}K
$T_{\epsilon=1}$	surface temperature computed with an emissivity of 1.0, ^{o}K
$\Delta T/\Delta t$	change in temperature with time, $^{o}K/sec$
ϵ	emissivity
2θ	angle between undisturbed X-ray and diffracted X-ray, deg
ρ	density, kg/m^3

Subscripts:

c	char
g	gases
p	virgin material
t	total

ABBREVIATIONS

HAHT	hypersonic arc-heated tunnel
HEAT	high-enthalpy arc tunnel

The letters α and β denote crystalline forms.

TEST FACILITIES

The models were tested in both the Langley 20-inch hypersonic arc-heated tunnel and the high-enthalpy arc tunnel at the Langley Research Center. These facilities are equipped with a conical nozzle composed of three segments which allow the test gases to be expanded to different exit conditions. The test gas is heated in both tunnels by its passage through an electric arc. The heated gas then expands through the nozzle until the desired exit condition is reached. Models are mounted on swing arms and are retracted from the test stream into a low-pressure region of the test section to prevent further oxidation of a hot test model. References 2 and 3 offer a concise description of these two facilities and the range of test conditions which may be attained.

MODELS

Material Model

The material model consisted of a sheath of test material mounted on a mild-steel shell. A test model is shown in figure 1 partly disassembled to illustrate the construction. The model diameter was 3.81 cm with nose thicknesses of 1.27 and 1.91 cm. The specific contour of the nose was selected to produce a uniform heating rate across a major portion of the front face of the model. The dimensions used to achieve the specific contour are shown in the figure 1 insert.

The material, designated E4A1, is composed of phenolic and silica hollow microspheres, silica fibers, and a room-temperature-vulcanizing silicone resin. The final density of the E4A1 used in this investigation was 633 kg/m^3 (39.5 lbm/ft^3) with a variation of ±0.6 percent. The percentages by weight of the different ingredients in E4A1 are listed in table I. The elemental analysis of this material is shown in table II.

Heating-Rate Models

Two models, which were thin-wall calorimeters, were used for the stagnation-point heating-rate determination. One model had the same dimensions and shape as the material models. This model was made of inconel alloy and is shown in figure 2.

The second heating-rate model had a 2.54-cm body diameter with a flat front face. This model was constructed from type 347 stainless steel and is shown in figure 3.

With both calorimeters, the relation

$$\dot{q} = \rho c_p l \frac{\Delta T}{\Delta t}$$

was utilized in the calculation of heating rate. The measured heating rates for the flat-face model were converted to heating rates for the material-model shape by the method described in reference 4.

Pressure Model

The pressure model was machined from copper to the exact dimensions of the material models. The model and the locations of the six pressure orifices are shown in figure 4. The model was water cooled to provide test times long enough for the pressures to reach a steady-state value.

TESTS

Conditions

The measured test parameters, stagnation-point pressure and heating rate, for the range of conditions are listed in tables III and IV. The calculated values of total stream enthalpy and peak shear on the face of the test models are also provided in the tables. Enthalpy was calculated by the method of Fay and Riddell (ref. 5). The shear distribution was calculated from the measured pressure distribution with the approximate method of Zoby (ref. 6). The free-stream Mach number varied from 3 to 8 for the entire range of test conditions.

Procedure

The tunnel was started, and a pressure model and calorimeter were inserted, successively, into the test stream until the test condition was established. After the test condition was established, the tunnel was turned off. Then the pressure probe was replaced with a material model, and the procedure listed below was followed:

(1) The material model was sealed in a low-pressure environment ($\approx 1 \times 10^{-3}$ atm) for approximately 30 minutes.

(2) The tunnel was started and transient conditions given time to settle out.

(3) The calorimeter was inserted into the test stream, and upon its withdrawal the material model was inserted into the stream and left until a loss of 0.50 to 0.75 cm of material had been accomplished. The time of withdrawal of the models which did not recede was based on a rapid rise in back-surface temperature.

(4) The charred model then cooled for approximately 15 minutes in the low-pressure environment (less than 7×10^{-3} atm) and was removed for examination.

During the exposure to the stream, the surface behavior was recorded on film by high-speed motion-picture cameras.

CHAR-ANALYSIS INSTRUMENTATION

The char layers were analyzed as to possible crystalline content by use of an X-ray diffractometer. This equipment displays diffracted X-ray intensity, determined by a Geiger-Müller ionization counter, against 2θ. The machine had just been alined and calibrated with a silicon standard. The calibration indicated that the machine was accurate in reading 2θ to within 1 percent of the actual value. Reference 7 provided information on sample preparation and general operation of an X-ray diffractometer, and served as a guide to procedure in powder X-ray diffraction techniques and interpretation of the data.

RESULTS AND DISCUSSION

Char Appearance

Models tested in air.- The models of silicone-resin-based material (E4A1) tested in air during this investigation formed char layers of three distinctly different types as the heating rate was varied from approximately 1.36 MW/m^2 to 10.2 MW/m^2 (120 to 900 Btu/ft^2-sec) and stagnation pressures from 0.016 atm to approximately 0.5 atm. At stagnation pressures near 0.6 atm a mechanical mode of char removal was observed. The change in appearance of the char layers may be observed in figure 5, and the appearance of the models which experienced mechanical char removal may be observed in figure 6.

In figure 7, the measured stagnation-point pressures are plotted against the stagnation-point heating rates for the material tests in an air test stream. The calculated lines of constant enthalpy and peak shear level are indicated. This plot is used to show the variation of char appearance with heating rate and to indicate the pressure and shear levels where mechanical char removal occurred.

At heating rates below approximately 1.48 MW/m^2 (130 Btu/ft^2-sec) over a range of pressures from 0.016 to 0.45 atm, the char layers formed were very hard and black with large cracks in the surface. This char-layer surface is shown in figure 5(a). The models exhibiting this type of char did not recede, but swelled to register a net gain in thickness.

At heating rates between approximately 1.81 MW/m^2 and 3.4 MW/m^2 (160 and 300 Btu/ft^2-sec), the char layer was coated with a glassy melt. The coating was brittle and flaked off easily to expose a gray sublayer. A typical surface of this type is illustrated in figure 5(b).

At heating rates greater than approximately 3.4 MW/m^2 and at stagnation pressures below approximately 0.6 atm, the char layers were smooth and gray in appearance. The

models receded uniformly and produced a relatively thin char layer with a char—virgin-material junction stronger than that produced at lower heating rates. Although the char was hard, some particles could be brushed from the surface easily. A typical char surface of this type is shown in figure 5(c).

Models tested in nitrogen.- The char surface layers formed in a nitrogen test stream at heating rates of approximately 4.1 MW/m^2 (360 Btu/ft^2-sec) and higher were very similar in appearance to the smooth gray char layers formed in air, except that the char surface layers of models tested in nitrogen were green. The tint of the models is attributed to silicon carbide crystals, which turn green on absorption of nitrogen.

Char and Virgin-Material Recessions

Mechanical failure.- At a pressure level of approximately 0.6 atm, the char layers of all but two models were lost mechanically. The mechanical removal was observed during the tests by studying the high-speed motion-picture film and film from the photographic optical pyrometer. At heating rates near 10.2 MW/m^2 a significant amount of the char layer was retained (see fig. 6(b)); however, mechanical removal was in the form of flakes of char missing around the front surface, especially near the corners. At heating rates below 7.6 MW/m^2 the mechanical failure was observed as the complete removal of the char layer over the major portion of the front face of the model and the exposure of virgin material. The appearance of a typical model of this type after testing is shown in figure 6(a).

From figure 7 it is obvious, at least for the region where a smooth gray char surface was formed, that all models tested at stagnation-point pressures of approximately 0.6 atm and greater failed mechanically. In the present range of test conditions, shear level did not indicate any correlation for the mechanical char failure observed.

Mechanical failure was also observed for two models at a pressure level of approximately 0.6 atm in the heating-rate region where black char was formed. However, data in this region are insufficient to attribute the failure to shear or pressure level.

Char recession in air streams.- The recession of the char surface was determined by measuring the length of a model before and after exposure to the test stream. A char-recession-rate parameter was calculated by dividing the change in length ΔL by the exposure time Δt. Determined in this manner the char-recession-rate parameter will always be less than the true steady-state recession rate of the surface. For reasonably long model test times or high recession rates, the difference between the char-recession-rate parameter and the true recession rate is small. The char-recession-rate parameter $\Delta L/\Delta t$ for each model tested is shown in table V.

The logarithm of the char-recession-rate parameter was plotted against the measured cold-wall heating rate as shown in figure 8. The data for the models which formed the gray char surfaces were fitted with a least-squares straight line. The resulting equation

$$\frac{\Delta L}{\Delta t} = 4.123 \times 10^{-2} \dot{q}^{1.189}$$

correlated the data well, the bulk of the data points being within ±10 percent of the fitted line. Since the char recession for the models forming the glassy-coated surfaces did not approach a steady-state condition, a recession-rate parameter would not approximate the actual char recession rate, and therefore no correlation with heating rate was attempted. Correlations of mass-loss rate with cold-wall heating rate have been previously reported for this type material. (See ref. 8.)

The measured char surface temperatures are also listed in table V. The values listed represent the constant level of surface temperature reached during the test. These temperatures were measured with a photographic optical pyrometer of the type described in reference 9. Since the emissivity of the char surface was not accurately known, an assumed emissivity of 1.0 was used in the reduction of the surface-temperature data. The correction curves in figure 9 can be used to correct these temperatures for assumed emissivities from 0.6 to 1.0.

A mass-loss-rate parameter was calculated for the models forming the gray char. This parameter is the product of the char-recession-rate parameter and the assumed char density of 212 kg/m^3. This value of char density was selected as an average between the high- and low-density extremes measured in reference 8. This value of char density is approximately one-third the density of the uncharred material. The mass-loss-rate parameters were plotted against the reciprocal of the measured surface temperatures corrected with an assumed emissivity of 0.75 (a value within the range of the measured emissivities of silica or silicon carbide). A pressure term was included to reduce the spread of the data. This correlation is shown in figure 10. The equation

$$\rho_c \frac{\Delta L}{\Delta t} = 20.79 \left(p_s/r\right)^{0.28} e^{-16117/T}$$

(where $r = 0.0424$ m) represents the linear least-squares fit of data points and is shown as the solid line in figure 10. The power of the pressure term used to reduce the spread of the data was arrived at by choosing the power which provided the minimum value for the sum of the squares of the deviations of the data points from the correlating line. The minimum value was obtained by using 0.28 for the power of $\left(p_s/r\right)$.

A correlation of this type has more merit than the correlation with heating rate in that it involves parameters measured at the model surface: pressure, recession, and temperature. This correlation involving temperature will also allow direct comparison with theoretical models which assume that the surface removal is the result of chemical reactions occurring in equilibrium at the model surface.

Char recession in nitrogen streams.- A limited number of models were also tested in nitrogen test streams. The char-recession-rate parameters $\Delta L/\Delta t$ for models tested in nitrogen are shown in figure 11 along with the data points for the tests in air again plotted against heating rate. At the lower heating rate (approximately 4.1 MW/m^2), the char-recession-rate parameter of a model tested in a nitrogen test stream was about one-fourth those observed in air. However, at heating rates of 10.0 MW/m^2 and higher the measured char-recession-rate parameters of models tested in nitrogen were nearly as large as those for models tested in air.

Since the char layers formed in nitrogen test streams were very similar in appearance, thickness, and consistency to those formed in air streams, the density was assumed to be 212 kg/m^3 and the emissivity 0.75. The mass-loss-rate parameter was calculated, and the term $\frac{\rho_c \frac{\Delta L}{\Delta t}}{(p_s/r)^{0.28}}$ was computed. This was plotted against the reciprocal of surface temperature as shown in figure 12. Although only a few data points were available, the term $\frac{\rho_c \frac{\Delta L}{\Delta t}}{(p_s/r)^{0.28}}$ for the models tested in nitrogen suggests a significantly higher dependence on temperature than suggested by the data for the models tested in air.

Virgin-material recession.- The virgin-material length after testing was determined from a sectioned model. A microscope with a reticle in the eyepiece was used for the measurement from the bond line to the char interface. The recession-rate parameter for the virgin material was calculated by dividing the difference between the original length and the lengths of the virgin material after testing by the test time. This was converted to a mass-loss-rate parameter for the virgin material by multiplying by the virgin-material density, 633 kg/m^3. The mass-loss-rate parameter for the virgin material is plotted against the model surface temperatures in figure 13. The solid line in this figure represents the data correlation (for the E4A1 material) from reference 8. The data points from the present study fall slightly higher than the correlation of reference 8 primarily because of the difference in the method of determining the mass-loss rates. In reference 8 the mass-loss rate of the virgin material was defined as the difference in mass loss of two models tested for different lengths of time at the same test condition divided by the difference in exposure time of the two tests. Since the method of reference 8 allows for char buildup and the method of the present study does not, the present

mass-loss-rate parameter should always be somewhat higher than the mass-loss rates of reference 8. The agreement of the present data with the correlation of reference 8 is relatively close; therefore, no correlation of the present data was attempted.

Chemical and X-Ray Diffraction Analysis of Char Layers

Because of the elemental composition of the silicone-resin-based ablation material, the formation of char surface layers containing different condensed species was expected. The variation of appearance of the char surface with heating rate offered further evidence that this was the case. The top 0.127 cm of char in the vicinity of the stagnation point was removed for analysis by powder X-ray diffraction techniques. This was done for each of the three different-appearing char layers.

The black chars formed at heating rates below 1.48 MW/m^2 were found to contain the crystalline form of silicon dioxide, α-cristobalite. A typical X-ray diffraction pattern for this type char layer is shown in figure 14(a). The same char samples were then reacted with hydrofluoric acid in an attempt to determine quantitatively the percent silicon dioxide in the char. The samples analyzed indicated that the amount of silicon dioxide in the char-layer samples ranged from 85 to 91 percent by weight. The remaining portion of the char sample was scanned again on the X-ray diffractometer. The samples were amorphous after the reaction, and a typical diffraction pattern is shown in figure 14(b).

The glassy-coated char layers formed at heating rates from 1.81 to 3.4 MW/m^2 were analyzed in two stages: First the melt coating was removed, powdered, and scanned on the X-ray diffractometer. Then approximately the next 0.127 cm beneath the melt layer was taken for analysis. The melt layer was found to be amorphous, but reacted with hydrofluoric acid. Therefore, the melt was assumed to be silicon dioxide. The layer of char beneath the melt contained α-cristobalite, and the pattern is shown in figure 15(a). After reaction of this layer with hydrofluoric acid, the residue was found to contain β-silicon carbide. The diffraction pattern is shown in figure 15(b). The amount of silicon dioxide removed from these chars ranged from 81 to 86 percent by weight. The silicon dioxide content may have been greater, but the sample became too small to work with.

The smooth gray char layers formed at heating rates above 3.4 MW/m^2 were found to contain β-silicon carbide. One of the better diffraction patterns for this type char formed in air is shown in figure 16(a). In general, the diffraction patterns of this type char indicated a higher intensity with increasing heating rate or a greater extent of the reaction between silicon dioxide and carbon. The char layer samples were still predominantly silicon dioxide. Approximately 81 percent by weight of the char sample was removed during reaction with hydrofluoric acid. Again the content was probably greater, but the sample became too small to work with.

The high percentage of silicon dioxide observed in the smooth gray char layers was the result of using the entire thickness of char in order to obtain enough material for analysis. The silicon carbide was believed to be a thin coating over the surface. The major portion of the silicon dioxide was probably located beneath the thin silicon carbide layer. At the measured surface temperatures for the models forming the smooth gray chars, any silicon dioxide at the surface would have been in a liquid state. Examination of the high-speed motion-picture film taken during the tests and the models after the tests did not yield evidence of a molten surface.

The X-ray diffraction pattern of a char layer taken from a model tested in a nitrogen test stream is shown in figure 16(b). The two char layers represented in figure 16 were formed at approximately the same pressure and heating rate. The higher intensity peaks for the char formed in the nitrogen test stream indicate a greater concentration of silicon carbide.

In summary, the char-analysis data have indicated that the char layers contain large percentages by weight of silicon dioxide. The char layers formed at low heating rates, below 1.48 MW/m^2, do not appear to have reactions between silicon dioxide and carbon occurring because of the absence of silicon carbide in the X-ray diffraction patterns.

Theoretical Analysis With Chemical Equilibrium

Analysis.- The equilibrium-surface-thermochemistry (EST) computer program described in reference 10 was used to predict the surface behavior of E4A1. The assumptions made in using the computer program were (1) complete chemical equilibrium of all reactions in a region near the char surface, (2) equal heat- and mass-transfer coefficients, and (3) occurrence of steady-state ablation. The inputs necessary to run the computer program were (1) the surface pressure, (2) the mass fraction of each element in the pyrolysis gas, char layer, and edge gas, and (3) the ratio of pyrolysis-gas and char mass-loss rates. Outputs from the computer program include (1) surface mass-loss rates as a function of temperature and pressure, and (2) the variation of surface condensed species with pressure, mass-loss rates, and temperature.

Since the models which formed the smooth gray char surface layers were believed to be approaching steady-state ablation by virtue of their relatively high recession-rate parameters and their thin char layers, it was believed that for these models, a realistic comparison with the equilibrium predictions was possible. The char density was not determined in the present study; however, a value, as explained earlier, of 212 kg/m^3 was assumed, which is approximately one-third the density of the virgin material. This yields a value of $\dot{m}_g/\dot{m}_c$ of 2 or, in terms of the computer inputs, a value of B_g'/B_c' of 2, where B_g' and B_c' are the pyrolysis-gas and char mass-loss rates, respectively,

made dimensionless by dividing by the heat-transfer coefficient corrected for gaseous injection. Arbitrary values of B_g' and B_c' were input to the computer so that B_g'/B_c' was always 2.

The elemental analysis of the virgin material is given in table II(a). The percentage of each element in the char layer was determined by assuming (based on the previously described X-ray diffraction studies) that the char layer was 85 percent by weight silicon dioxide and 15 percent by weight carbon. These values are given in table II(b). Since the weight of each element in the virgin material and in the char was known, the weight and therefore percentage of each element in the pyrolysis gases was determined. These values are given in table II(c). The edge gases were air and pure nitrogen.

The remaining input to the computer program was the surface pressure. The chemical-equilibrium calculation was performed for surface pressures of 0.01, 0.1, and 1.0 atm for air and 0.1 and 1.0 atm for nitrogen to cover the range of the experimental values.

The output B_c' values were converted into a surface mass loss $\dot{m}_c/\sqrt{p_s/r}$ in the manner described in reference 1 to allow a straightforward comparison with the experimental data. This term is derived by use of the relation from reference 11

$$h_o \approx K\sqrt{p_s/r}$$

where $K = 0.0461$ for air and 0.431 for nitrogen. Since B_c' is defined as

$$B_c' = \frac{\dot{m}_c}{h}$$

then,

$$B_c' = \frac{\dot{m}_c}{K\sqrt{p_s/r}(h/h_o)}$$

which rearranges to become

$$\frac{\dot{m}_c}{\sqrt{p_s/r}} = KB_c'(h/h_o)$$

The term h/h_o is the correction in the heat-transfer coefficient for mass injection and was computed with the linear approximation of reference 12 in the form

$$\frac{h}{h_o} = \frac{1}{1 + 0.6B_t'}$$

where $B_t' = B_c' + B_g'$. The correction factor is close to the exact solution indicated in reference 12 for air-to-air injection as long as B_t' does not exceed a value of approximately 2.5.

Comparison of experimental and theoretical results.- In figure 17 the mass-loss-rate term $\dot{m}/\sqrt{p_s/r}$ is plotted against surface temperature. The solid lines represent the theoretically calculated mass-loss-rate terms in air at surface pressures of 0.01, 0.1, and 1.0 atm. The dashed portions of the curves represent the region in which the data were extrapolated because of the small change in $\dot{m}/\sqrt{p_s/r}$ with temperature. The char surfaces represented by these lines are predominantly silicon carbide. The symbols represent the experimentally measured mass-loss-rate terms at the measured surface temperatures. The char surfaces for a number of the models represented in figure 17 were found to contain silicon carbide. The surface temperatures for this plot were based on an assumed emissivity of 0.75. The surface pressures for the experimental points are listed on the plot.

The agreement between the theoretical results and experimental results was reasonably good in view of the possible errors in the experimental surface-temperature data. The estimated accuracy of the photographic pyrometer used in this investigation is from ±3 to ±5 percent over the temperature range of the present tests. Applying this error to the data points in figure 17 would shift the data to a much better agreement in pressure level, except for the five points below the theoretical curves. The assumed emissivity may also contribute to an error in surface temperature. A difference of ±0.1 in emissivity could cause a difference in temperature of as much as ±1.5 percent.

There are also uncertainties in the theoretical analysis resulting from assumptions made. The char density was assumed as an average of the measured extremes in reference 8, and could possibly be as much as ±15 percent in error. A different char density, and therefore a different $\dot{m}_g/\dot{m}_c$, would shift the location of the theoretical curves vertically in figure 17. The assumptions used should provide a representative set of theoretical results.

The mass-loss-rate term in nitrogen is plotted in figure 18 against surface temperature. The solid lines represent the computed results for pressures of 0.1 and 1.0 atm. The surface at these pressures was predicted to be silicon carbide also. The same assumptions for the equilibrium solution with air as the edge gas were also made with nitrogen as the edge gas. The symbols on the plot represent the results of tests made in a nitrogen stream. The agreement of the theoretical and experimental data is again believed reasonably good. If the same errors possible in air because of the optical-pyrometer equipment and assumed emissivity could be minimized, better agreement in pressure level could possibly be achieved. The theoretically predicted char surface

species and the species determined experimentally were again in agreement. The greater dependence of the mass-loss-rate term on surface temperature may be observed by the nearly vertical lines in figure 18. This observation was suggested in the discussion of the experimental results in figure 12.

The correlation for the test results in air (fig. 10) indicated a different pressure dependence than is shown in the theoretical equilibrium solution of figure 17. When the experimental correlation

$$\frac{\rho_c \frac{\Delta L}{\Delta t}}{\left(p_s/r\right)^{0.28}} = 20.79e^{-16117/T}$$

was converted to the form plotted in figure 17 by multiplication of each side by $1/\left(p_s/r\right)^{0.22}$ the correlation then became

$$\frac{\rho_c \frac{\Delta L}{\Delta t}}{\left(p_s/r\right)^{0.5}} = 20.79\left(p_s/r\right)^{0.22} e^{-16117/T}$$

A comparison of the experimental correlation with the equilibrium solution is shown in figure 19. The constant-pressure lines agree very well, except for the lack of a plateau in the experimental results, which was indicated at approximately 0.024 $kg/m^{3/2}$-sec-$atm^{1/2}$ in the theoretical equilibrium solution. However, since the experimental data used in obtaining the correlation had values of the mass-loss term equal to or greater than 0.012 $kg/m^{3/2}$-sec-$atm^{1/2}$, the lower portion of the experimental correlation curves must be considered as an extrapolation which may or may not be physically meaningful. This portion is indicated by the dashed lines below 0.012 $kg/m^{3/2}$-sec-$atm^{1/2}$.

Since the models which formed the glassy surface layers did not approach steady-state ablation, no quantitative agreement with the outputs from the equilibrium-surface-thermochemistry program could be obtained. At low mass-loss rates the computer program did indicate that the surface species would be predominantly silicon dioxide. Thus in a qualitative sense, agreement between the experimental results and theoretical results was achieved, in that silicon dioxide was identified in experimentally produced chars.

SUMMARY OF RESULTS

A composite ablation material containing a silicone-resin base, silica fibers, and phenolic and silica hollow microspheres has been subjected to a wide range of test conditions to study its charring behavior. This material was developed at the Langley

Research Center and is designated E4A1. The ablation tests were carried out in both the Langley 20-inch hypersonic arc-heated tunnel and the high-enthalpy arc tunnel at the Langley Research Center at stagnation-point pressures ranging from 0.016 to 1.3 atm and heating rates ranging from 1.34 MW/m^2 to 14.8 MW/m^2 in air and nitrogen test streams. The resulting char layers were analyzed qualitatively by powder X-ray diffraction techniques to determine the chemical species present. Some quantitative measurements of char silicon dioxide content were obtained. Theoretical chemical-equilibrium predictions of char-layer constituents and surface mass removal were made and compared with the experimental results. The results of this investigation are

1. The resulting char-layer surfaces changed considerably in appearance as heating rates (and hence char surface temperatures) were increased. At heating rates from approximately 1.34 to 1.48 MW/m^2, the char layers were black with large surface cracks and did not recede but swelled to register a net gain in thickness. At heating rates between approximately 1.81 and 3.4 MW/m^2, the char layers were coated with a glassy melt. At heating rates above 3.4 MW/m^2, the char layers were thin, smooth and gray in appearance, and receded uniformly. At these higher heating rates the models appeared to approach steady-state ablation.

2. In the heating-rate region where a smooth gray char layer was formed, all models tested at stagnation-point pressures of 0.6 atm or greater exhibited mechanical failure. In the range of test conditions for these tests, shear level did not appear responsible for the mechanical failure. Models subjected to higher heating rates (approximately 10 MW/m^2) with stagnation-point pressures of 0.6 atm or greater did not exhibit char failure as drastic as at the lower heating rates.

3. Two correlations of the experimental ablation data were obtained. The surface recession-rate parameter $\Delta L/\Delta t$ was correlated against the cold-wall heating rate $\dot{q}$ to the model. The equation for the least-squares fit of a line to this data is

$$\frac{\Delta L}{\Delta t} = 4.123 \times 10^{-2}\, \dot{q}^{1.189}$$

where $\Delta L/\Delta t$ is in mm/sec and $\dot{q}$ in MW/m^2. The bulk of the data fell within ±10 percent of the fitted line.

A second correlation was obtained between the experimental surface mass-loss-rate parameters $\rho_c \frac{\Delta L}{\Delta t}$ and the measured surface temperatures and pressures. The equation for this correlation is

$$\rho_c \frac{\Delta L}{\Delta t} = 20.79\left(p_s/r\right)^{0.28} e^{-16117/T}$$

where the char density ρ_c times the recession-rate parameter $\Delta L/\Delta t$ is in kg/m^2-sec; the stagnation-point pressure p_s is in atm; the surface temperature T is in ^oK; and the effective hemispherical nose radius r is in meters.

4. Chemical and X-ray diffraction analyses showed that the chars formed at heating rates of 1.34 to 1.48 MW/m^2 contained from 85 to 91 percent (by weight) silicon dioxide with a significant portion in the form of α-cristobalite. The chars formed at heating rates from 1.81 to 3.4 MW/m^2 had a surface melt layer which was found to be amorphous silicon dioxide. The char beneath the melt layer was found to be 81 to 86 percent SiO_2 (again α-cristobalite was detected) and contained small quantities of silicon carbide. The chars produced at heating rates greater than 3.4 MW/m^2 contained approximately 81 percent SiO_2 and significant amounts of SiC. Because the peak intensity in the X-ray diffraction pattern for SiC increased with increasing heating rate, a greater extent of the reaction between silicon dioxide and carbon was indicated.

5. Surface mass-loss rates as a function of temperature and pressure were calculated for the models tested in air and nitrogen at high heating rates. Steady-state ablation and chemical equilibirum in reactions at the ablator surface were assumed for these calculations. The comparison between the theoretical results and the experimental results for air and nitrogen was reasonably good. In both air and nitrogen test streams, the predicted surface condensed species was silicon carbide, which was the species identified in the experimentally produced chars.

The models which formed the glassy surface coating could not be compared with the chemical-equilibrium results. This was primarily because of their failure to approach steady-state ablation. The equilibrium solutions did indicate that for low mass-loss rates the surface would be predominately silicon dioxide. The models which formed the glassy surface, believed to be silicon dioxide because of the reaction of the coating with hydrofluoric acid, did exhibit low mass-loss rates.

Langley Research Center,
National Aeronautics and Space Administration,
Hampton, Va., August 19, 1970.

REFERENCES

1. Wakefield, Roy M.; Lundell, John H.; and Dickey, Robert R.: The Effects of Oxygen Depletion in Gas-Phase Chemical Reactions on the Surface Recession of Charring Ablators. AIAA Pap. No. 68-302, Apr. 1968.

2. Midden, Raymond E.; and Cocke, Bennie W., Jr.: Description and Initial Calibration of the Langley 20-Inch Hypersonic Arc-Heated Tunnel. NASA TN D-4653, 1968.

3. Wells, William L.: Description of the High-Enthalpy Arc Tunnel at the Langley Research Center Including Test-Stream Conditions at Selected Operating Points. NASA TN D-5295, 1969.

4. Zoby, Ernest V.; and Sullivan, Edward M.: Effects of Corner Radius on Stagnation-Point Velocity Gradients on Blunt Axisymmetric Bodies. NASA TM X-1067, 1965.

5. Fay, J. A.; and Riddell, F. R.: Theory of Stagnation Point Heat Transfer in Dissociated Air. J. Aeronaut. Sci., vol. 25, no. 2, Feb. 1958, pp. 73-85, 121.

6. Zoby, Ernest V.: Approximate Relations for Laminar Heat-Transfer and Shear-Stress Functions in Equilibrium Dissociated Air. NASA TN D-4484, 1968.

7. Klug, Harold P.; and Alexander, Leroy E.: X-Ray Diffraction Procedures For Polycrystalline and Amorphous Materials. John Wiley & Sons, Inc., c.1954.

8. Hiester, Nevin K.; and Clark, Carroll F.: Comparative Evaluation of Ablating Materials in Arc Plasma Jets. NASA CR-1207, 1968.

9. Exton, Reginald J.: Theory and Operation of a Variable Exposure Photographic Pyrometer Over the Temperature Range 1800° to 3600° F (1255° to 2255° K). NASA TN D-2660, 1965.

10 Kendall, Robert M.; Rindal, Roald A.; and Bartlett, Eugene P.: A Multicomponent Boundary Layer Chemically Coupled to an Ablating Surface. AIAA J., vol. 5, no. 6, June 1967, pp. 1063-1071.

11. Zoby, Ernest V.: Empirical Stagnation-Point Heat-Transfer Relation in Several Gas Mixtures at High Enthalpy Levels. NASA TN D-4799, 1968.

12. Swann, Robert T.; Pittman, Claud M.; and Smith, James C.: One-Dimensional Numerical Analysis of the Transient Response of Thermal Protection Systems. NASA TN D-2976, 1965.

TABLE I.- ABLATION-MATERIAL INGREDIENTS

[Catalyst, 1 percent of resin]

Ingredient	Percent by weight
Silicone resin (RTV-602)	73
Silica microspheres (hollow)	11
Phenolic microspheres (hollow)	10
Silica fibers	4
Silicone fluid	2
Total	100

TABLE II.- ELEMENTAL COMPOSITION OF E4A1 VIRGIN MATERIAL, CHAR, AND PYROLYSIS GASES

(a) Virgin material (measured)

Element	Percent by weight
Carbon	30.35
Oxygen	31.71
Hydrogen	6.47
Nitrogen	.11
Silicon	31.36
Total	100.00

(b) Char (assumed)

Element	Percent by weight
Carbon	15.0
Oxygen	45.3
Silicon	39.7
Total	100.0

(c) Pyrolysis gases (calculated from (a) and (b))

Element	Percent by weight
Carbon	44.82
Hydrogen	11.21
Nitrogen	.34
Silicon	21.85
Oxygen	21.78
Total	100.00

TABLE III.- TEST CONDITIONS FOR CHAR MODELS NOT EXHIBITING MECHANICAL FAILURE

(a) Tests in air stream

Test	Measured parameters		Calculated parameters	
	p_s, atm	$\dot{q}$, MW/m^2	Enthalpy, MJ/kg	Shear, kN/m^2
Models forming black char layers				
1	0.016	1.50	22.7	<0.432
2	.057	1.46	11.8	<.432
3	.445	1.44	4.24	.624
4	.445	1.46	4.24	.624
Models forming glassy-coated char layers				
5	0.059	2.21	17.4	<0.624
6	.109	1.84	11.6	<.624
7	.109	2.03	11.9	<.624
8	.333	3.30	11.4	.767
9	.490	2.63	7.45	.720
10	.490	2.66	7.45	.720
11	.606	2.45	6.51	.815
12	.606	2.52	6.51	.815
Models forming gray char layers				
13	0.076	3.62	24.9	<0.624
14	.091	4.13	25.6	<.624
15	.1185	3.18	17.5	<.624
16	.1185	3.18	17.5	<.624
17	.1185	3.42	19.1	<.624
18	.1185	3.76	21.0	<.624
19	.273	8.50	31.7	<1.10
20	.342	4.75	16.6	.881
21	.342	6.60	21.8	.945
22	.411	10.2	31.4	-----
23	.442	7.08	20.2	1.05
24	.442	7.60	20.2	1.05
25	.442	7.25	20.2	1.05
26	.469	3.64	10.5	.815
27	.469	3.99	10.5	.815
28	.516	8.30	23.3	-----
29	.592	9.40	24.4	1.39

(b) Tests in nitrogen stream

Test	Measured parameters		Calculated parameters	
	p_s, atm	$\dot{q}$, MW/m^2	Enthalpy, MJ/kg	Shear, kN/m^2
30	0.0902	4.18	24.6	-----
31	.399	10.00	27.9	-----
32	.592	14.60	33.5	-----
33	.606	14.75	33.5	
34	.634	11.24	25.1	-----

TABLE IV.- TEST CONDITIONS FOR MODELS EXHIBITING MECHANICAL FAILURE

Measured parameters		Calculated parameters	
p_s, atm	$\dot{q}$, MW/m^2	Enthalpy, MJ/kg	Shear, kN/m^2
0.590	1.36	3.54	0.72
.590	1.34	3.54	.72
.616	5.36	12.60	1.10
.616	5.25	12.60	1.10
.615	7.36	17.50	1.24
.615	7.34	17.50	1.24
.605	10.20	23.60	1.39
.605	10.00	23.60	1.39
.642	12.00	28.00	1.48
.900	10.90	22.10	1.65
1.000	8.21	15.90	1.58
1.300	7.30	12.50	1.61

TABLE V.- MEASURED SURFACE RECESSION AND TEMPERATURES

Test	Model recession			Surface temperature, ^{o}K, for –	
	ΔL, mm	Test time, sec	ΔL/Δt, mm/sec	$\epsilon = 1.0$	$\epsilon = 0.75$
Tests in air stream					
1	0	129	----	1922	1970
2	0	110	----	1979	2030
3	0	41.5	----	2020	2080
4	0	38.1	----	2020	2080
5	3.51	100	0.035	1885	1930
6	1.27	108	.012	2095	2150
7	.76	45.0	.017	2115	2170
8	6.15	33.6	.183	2218	2280
9	2.21	36.0	.062	2210	2275
10	4.78	46.4	.103	2257	2325
11	.152	30.6	.005	2090	2148
12	-----	----	----	----	----
13	4.01	27.5	.146	2422	2490
14	6.94	25.0	.277	2582	2660
15	11.29	63.0	.179	2378	2445
16	5.91	42.0	.141	2395	2460
17	5.97	30.0	.199	2450	2520
18	12.70	59.0	.215	2395	2460
19	11.86	25.0	.475	2665	2750
20	5.84	23.3	.251	2325	2395
21	9.44	23.8	.397	2450	2520
22	12.11	21.1	.575	2592	2670
23	12.69	31.0	.410	2537	2610
24	10.15	20.7	.491	2595	2675
25	4.95	12.3	.403	2557	2625
26	4.24	20.5	.207	2320	2390
27	3.38	18.0	.188	2280	2345
28	8.89	15.0	.592	----	----
29	10.59	16.2	.653	2810	2900
Tests in nitrogen stream					
30	1.52	25.0	.061	2590	2668
31	12.21	20.9	.584	2685	2777
32	12.32	15.7	.785	----	----
33	13.32	15.4	.866	2645	2735
34	8.66	16.0	.541		

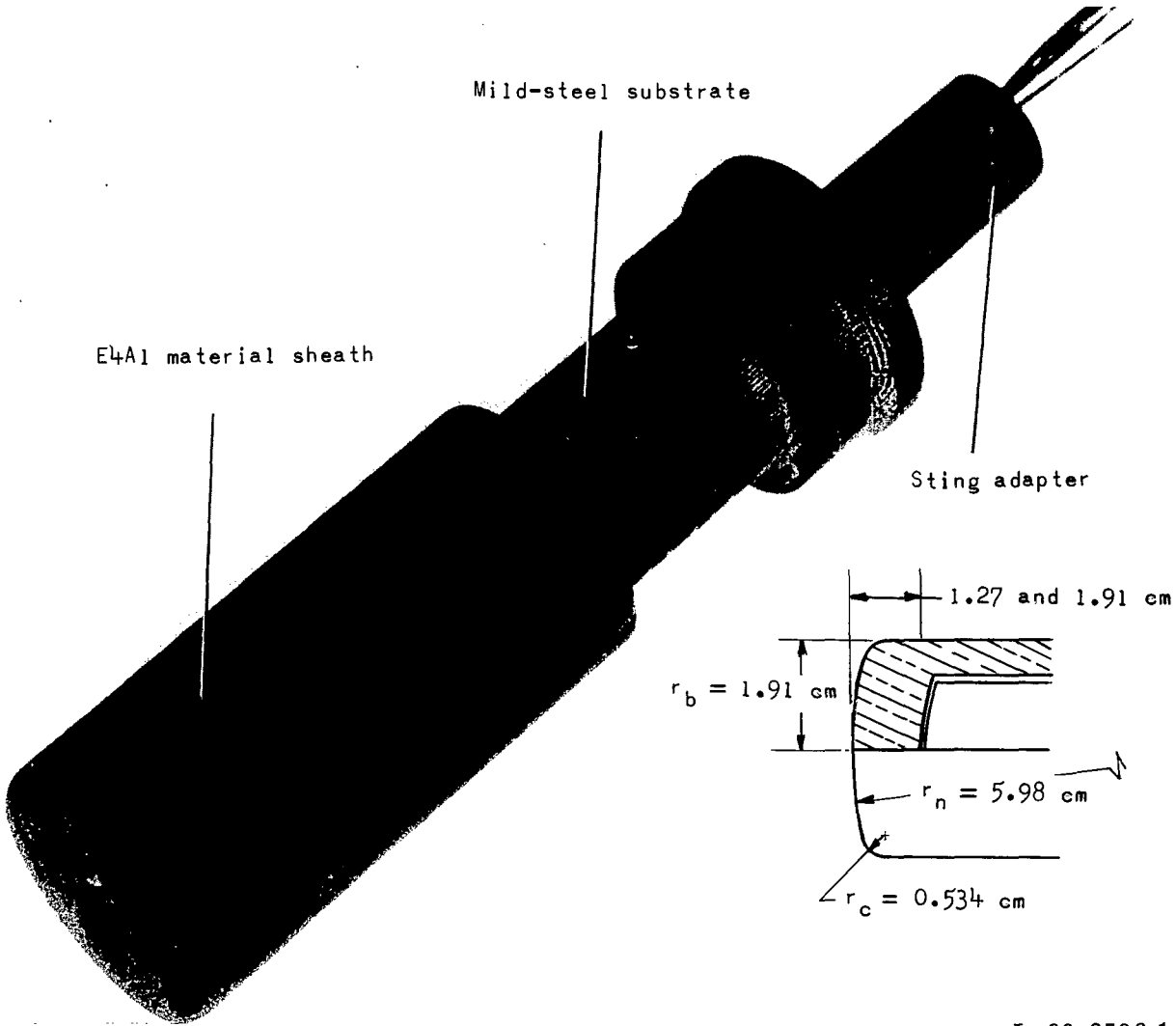

Figure 1.- Disassembled view of material test model with dimensions shown in insert.

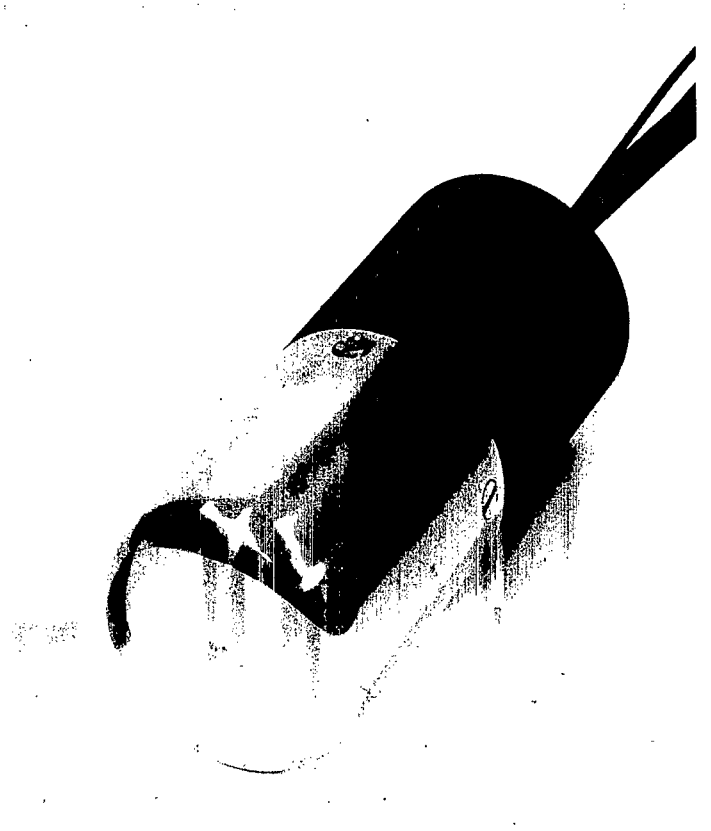

Point	s/r_b
①	0
②	.41
③	.61
④	.83
⑤	1.18
⑥	1.56
⑦	2.06
⑧	2.54

Nominal wall thickness, 0.127 cm

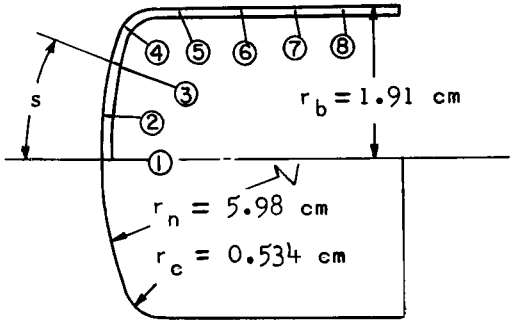

L-66-8137

Figure 2.- Heating-rate-distribution model.

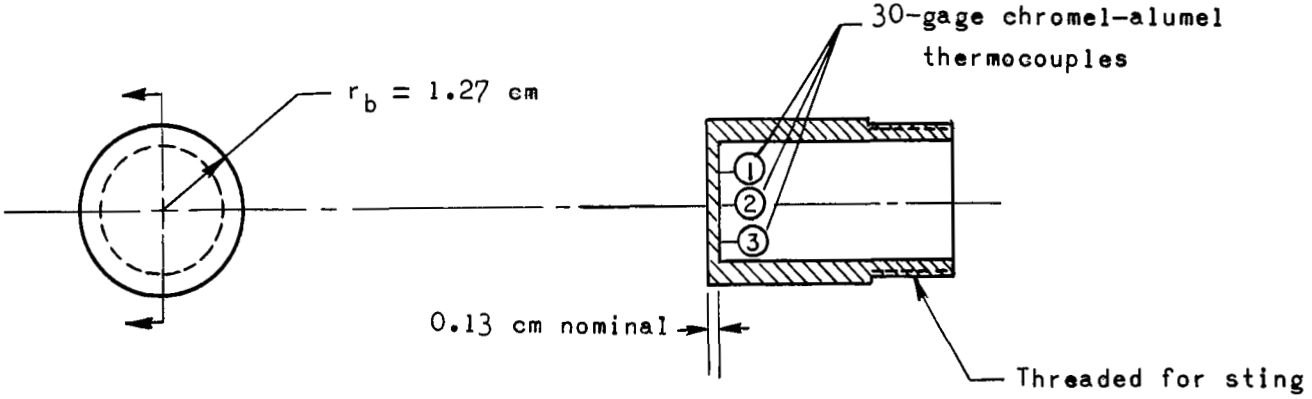

Figure 3.- Stagnation-point heating-rate model.

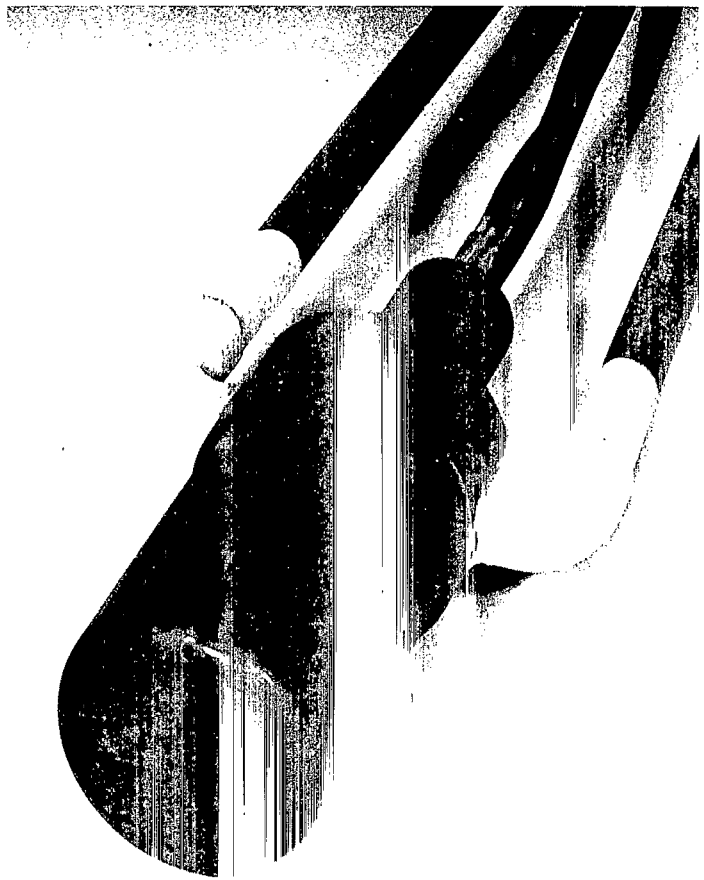

Point	s/r_b
①	0
②	.41
③	.71
④	.85
⑤	1.07
⑥	1.48

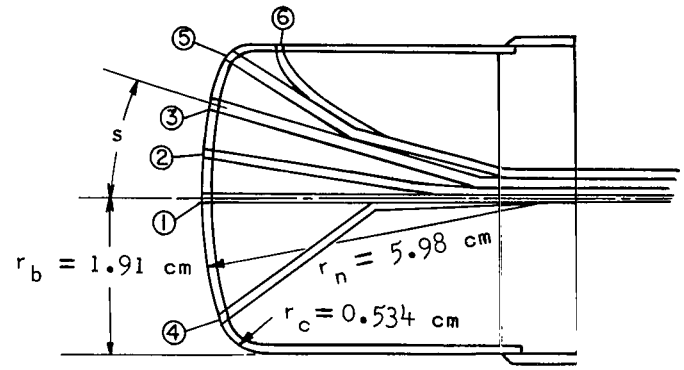

L-66-8140

Figure 4.- Pressure-distribution model.

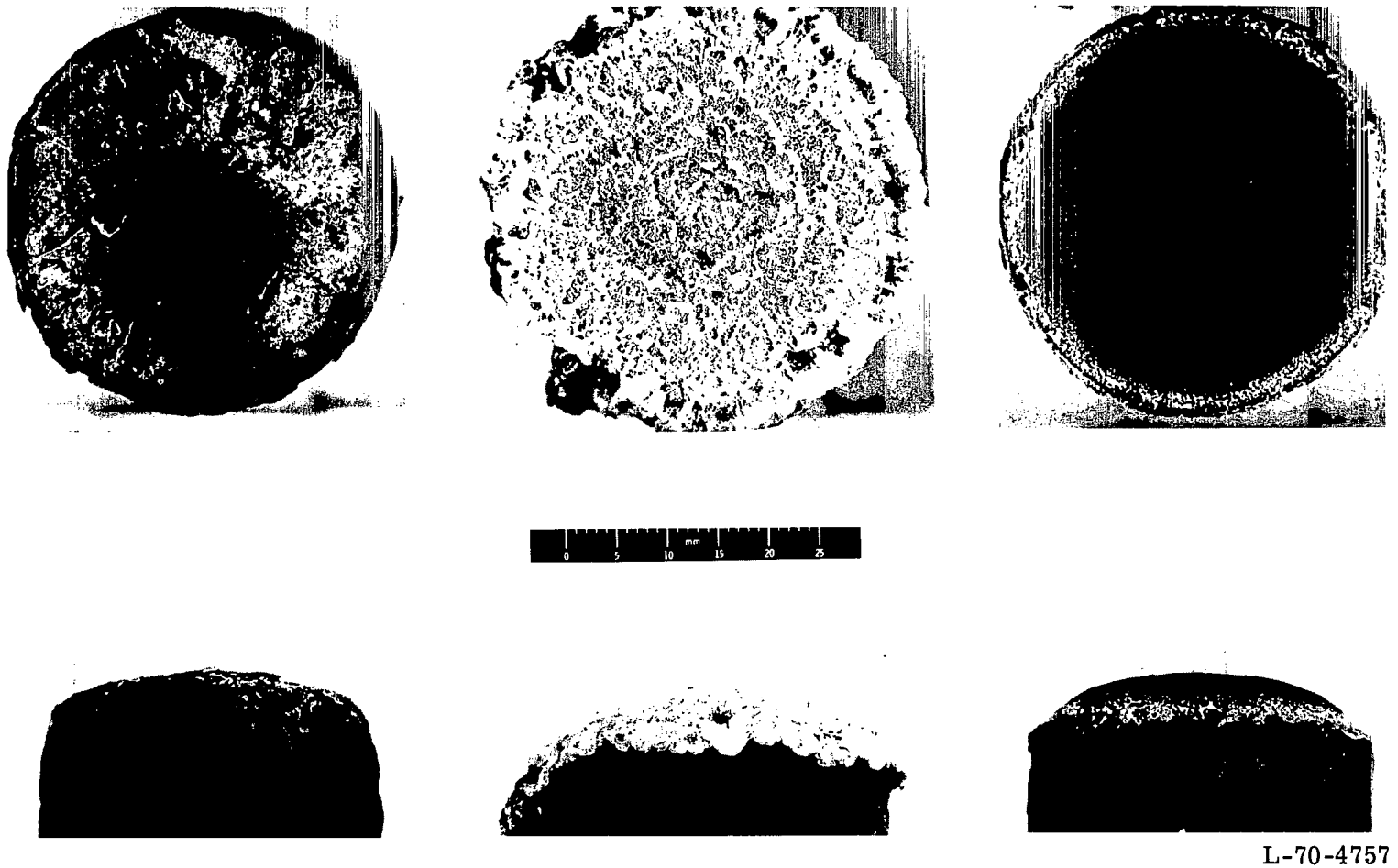

(a) Black char. (b) Glassy-coated char. (c) Gray char.

Figure 5.- Typical front and side views of charred models illustrating the three different surfaces formed in air.

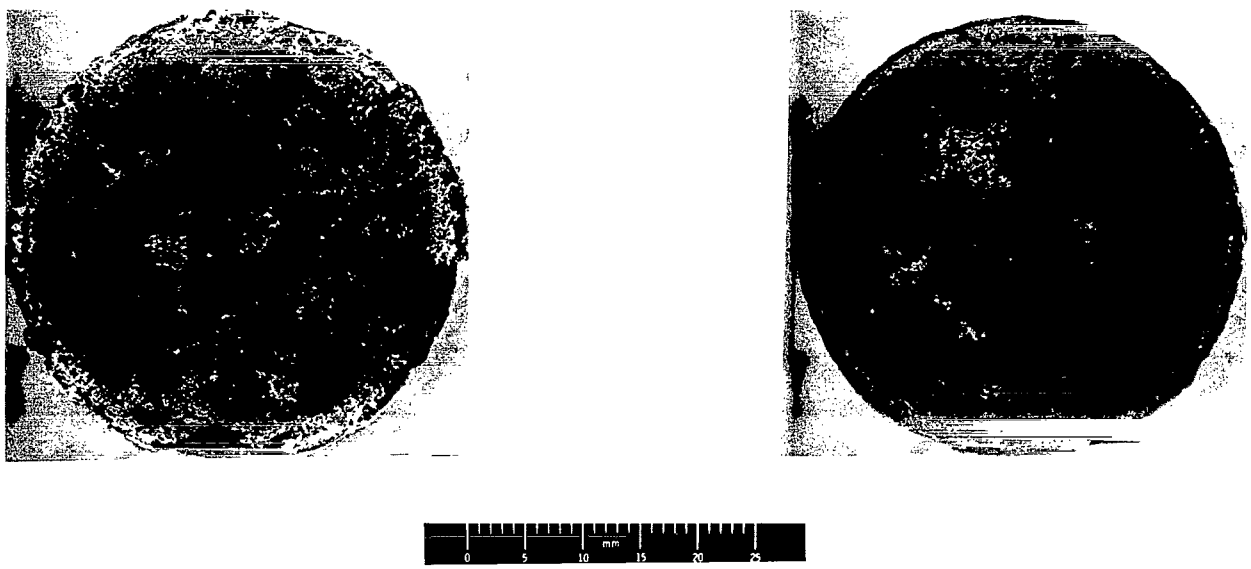

L-70-4758

(a) Char failure at heating rates below 7.6 MW/m^2.

(b) Char failure at heating rates near 10.2 MW/m^2.

Figure 6.- Typical front and side views of models which exhibited mechanical char failure.

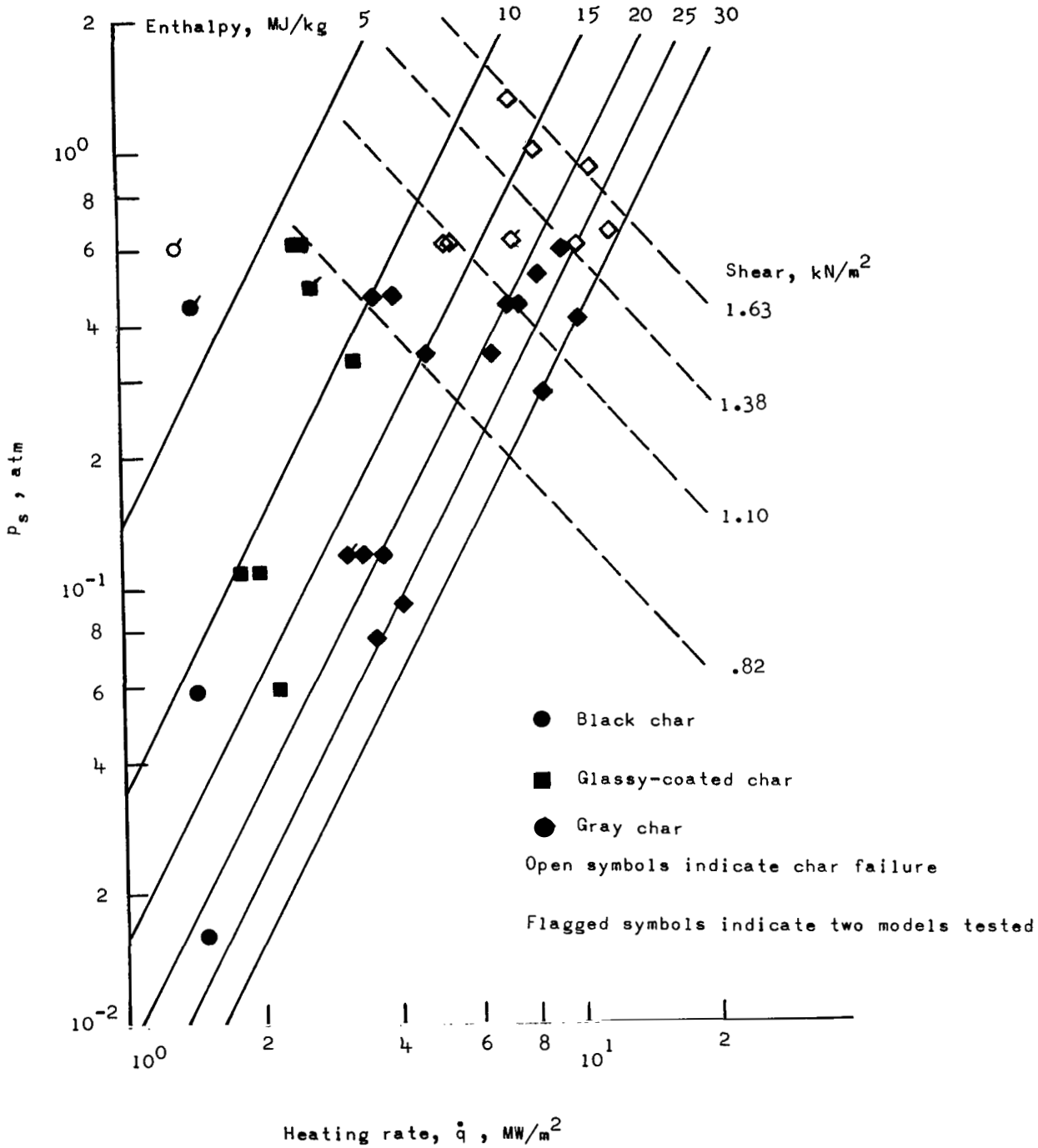

Figure 7.- Effect of shear and pressure on mechanical removal of char layer.

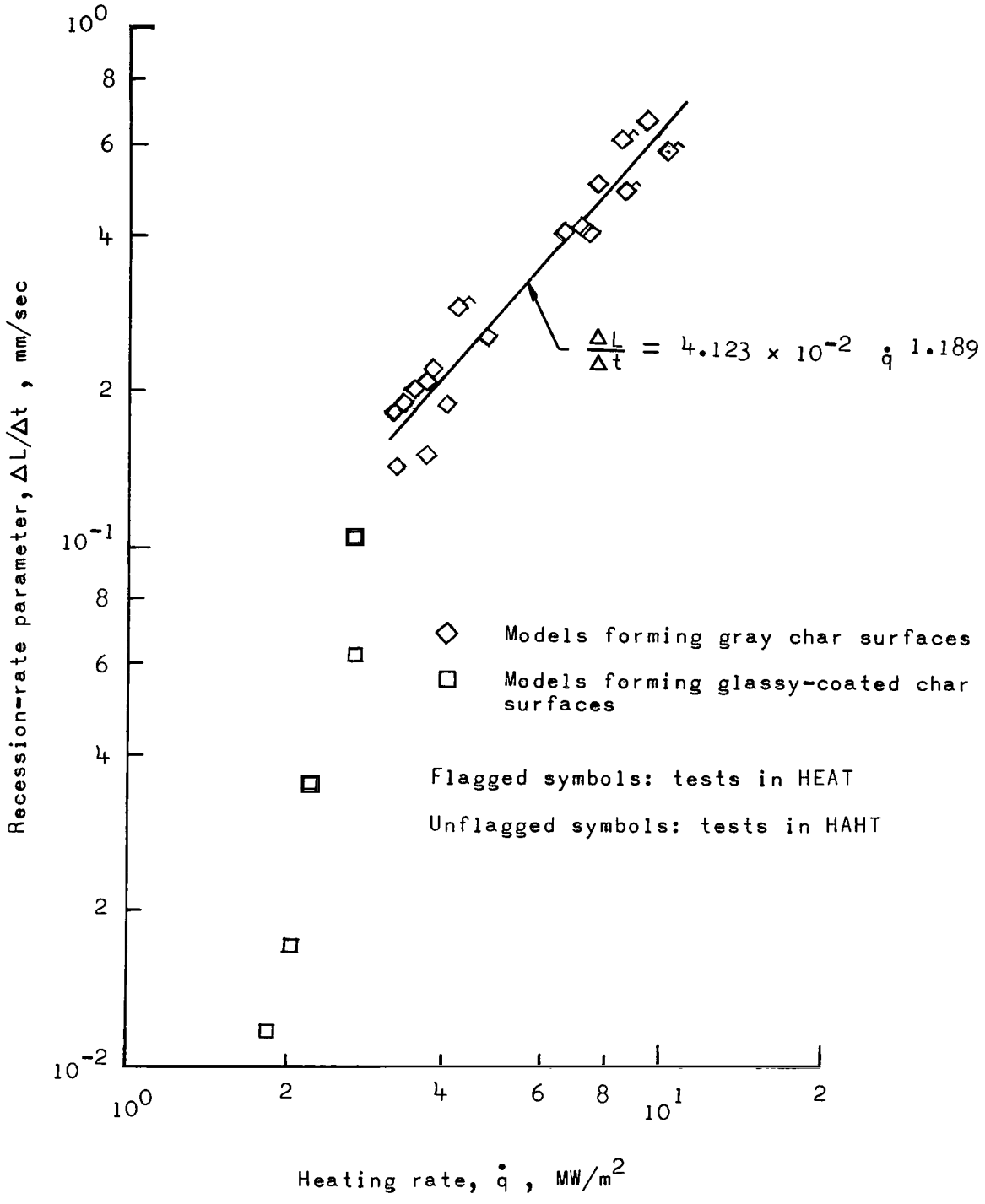

Figure 8.- Correlation of char recession-rate parameter with heating rate for models tested in air.

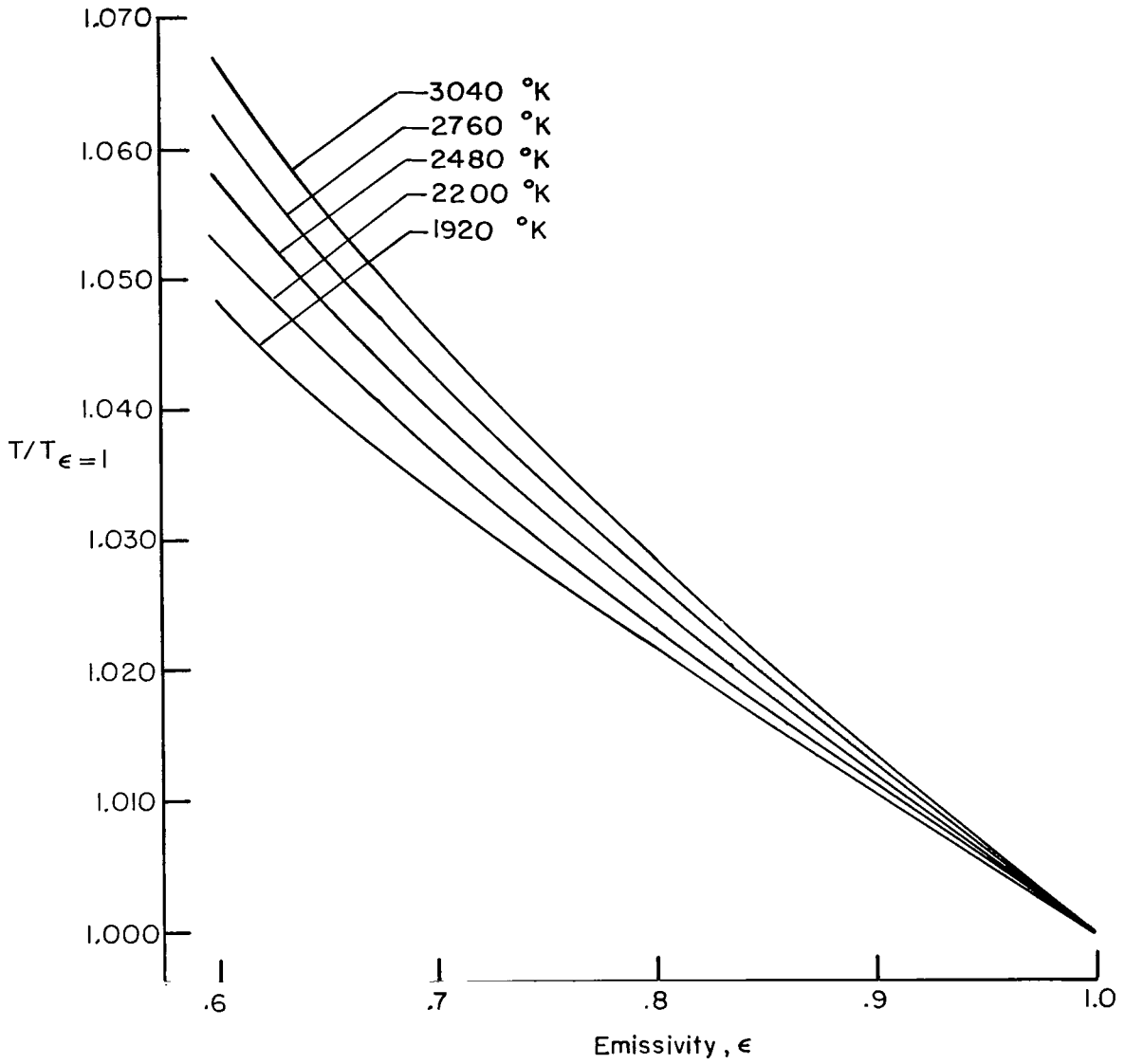

Figure 9.- Curves for correcting measured surface temperatures from the optical pyrometer for different emissivities.

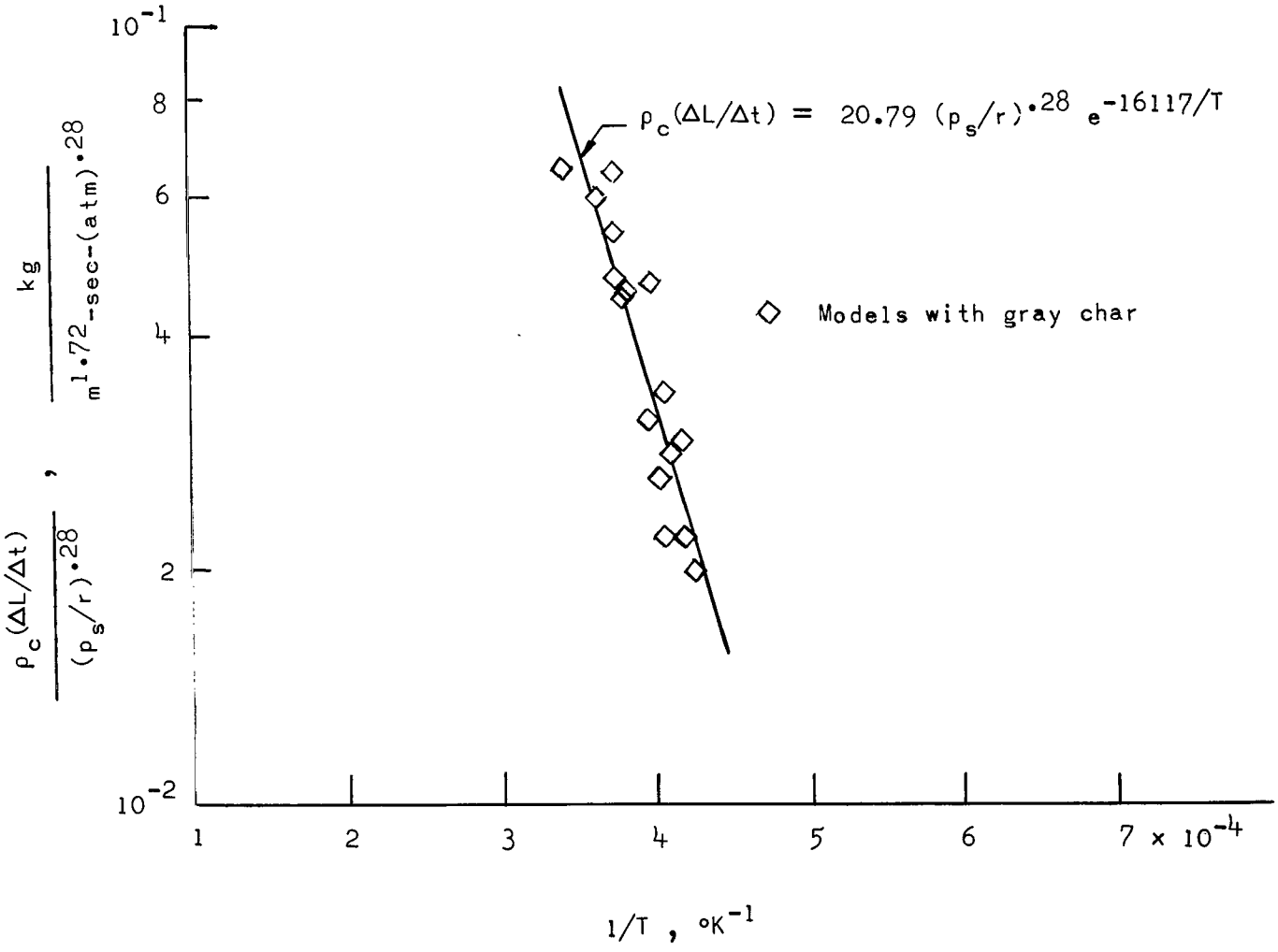

Figure 10.- Correlation of mass-loss-rate parameter with surface temperature for models tested in air. Surface temperatures corrected with an assumed emissivity of 0.75.

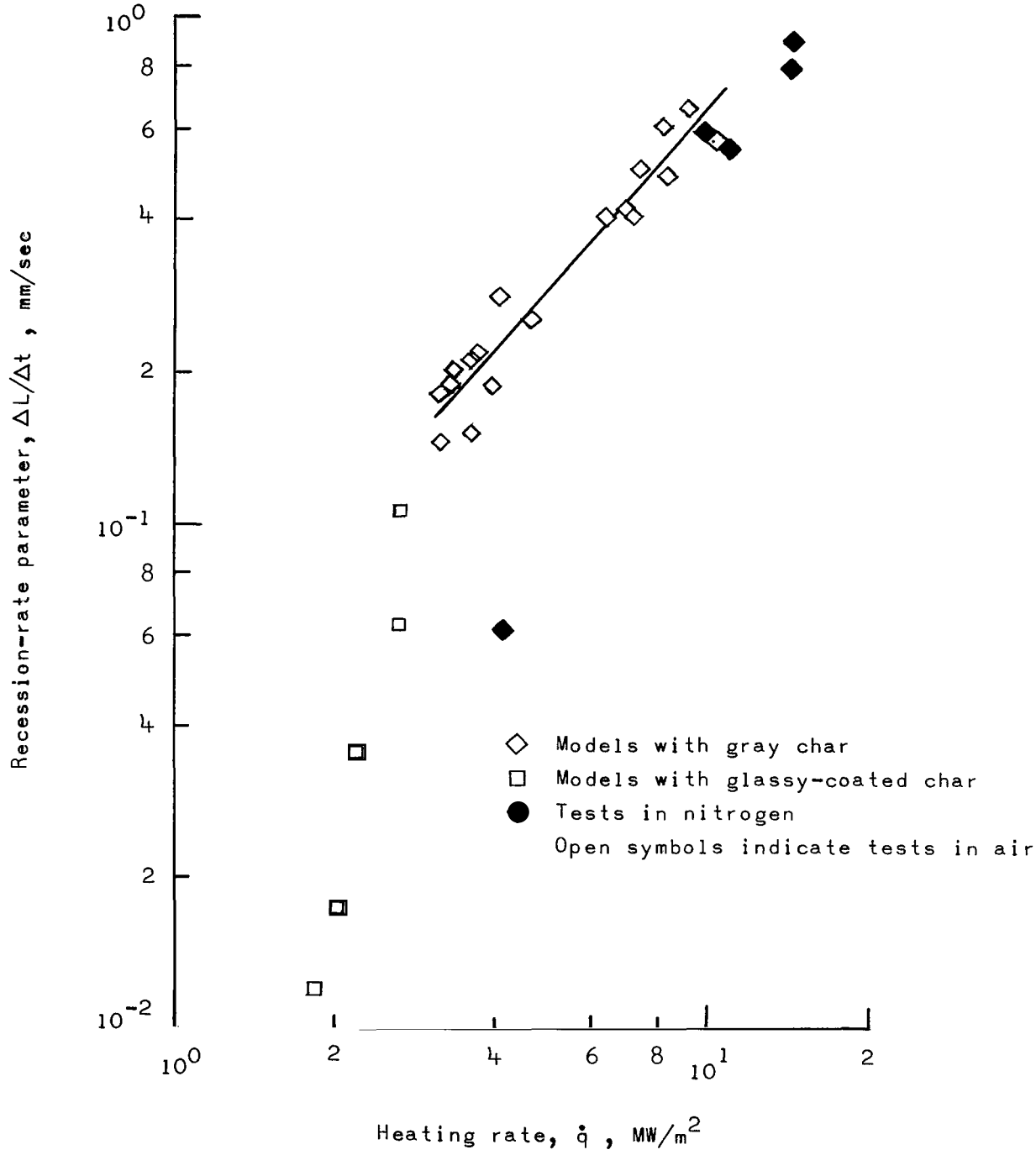

Figure 11.- Comparison of char surface recession in air and nitrogen streams based on heating rates.

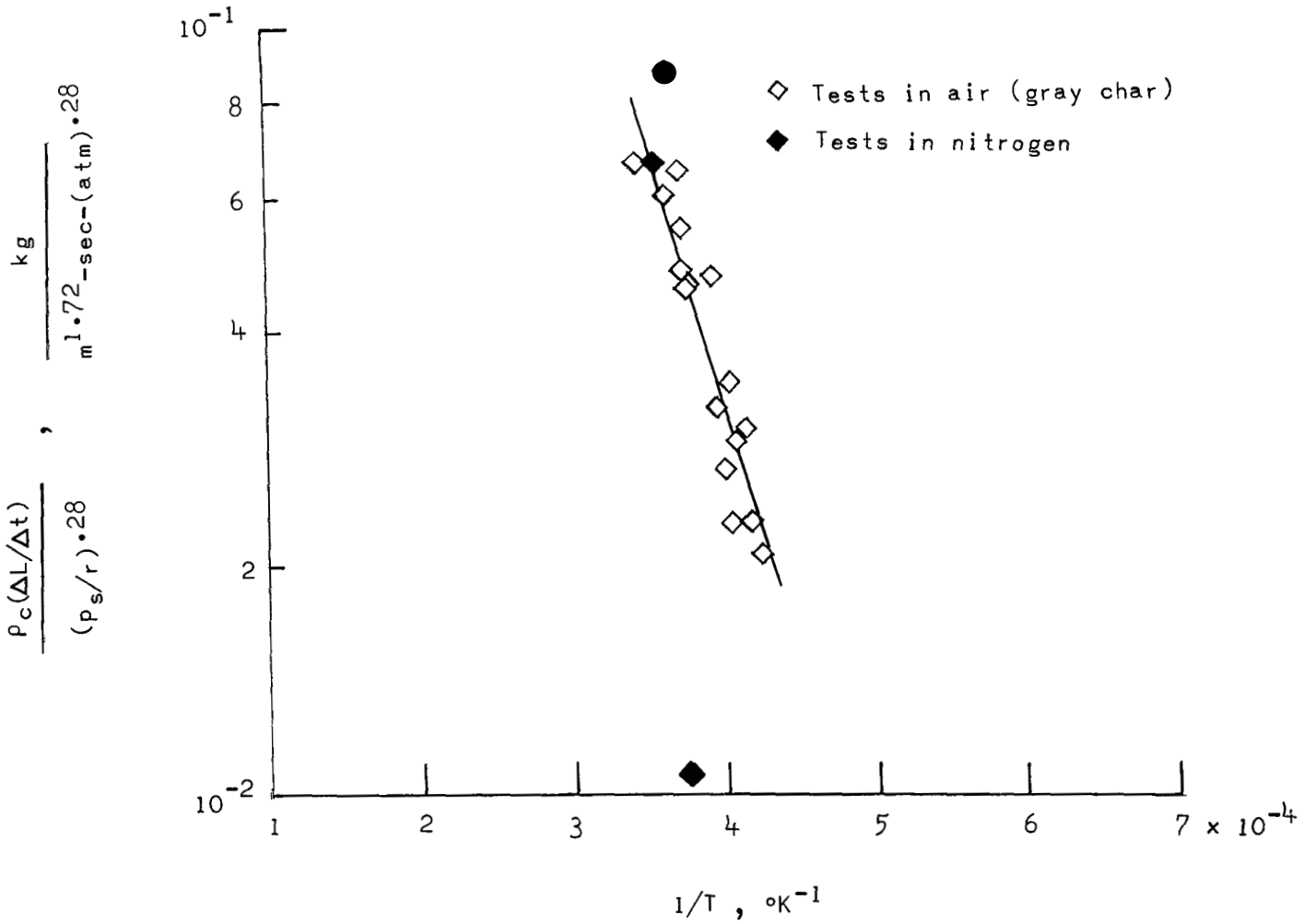

Figure 12.- Comparison of char mass removal in air and nitrogen streams based on surface temperature. Surface temperatures corrected with an assumed emissivity of 0.75.

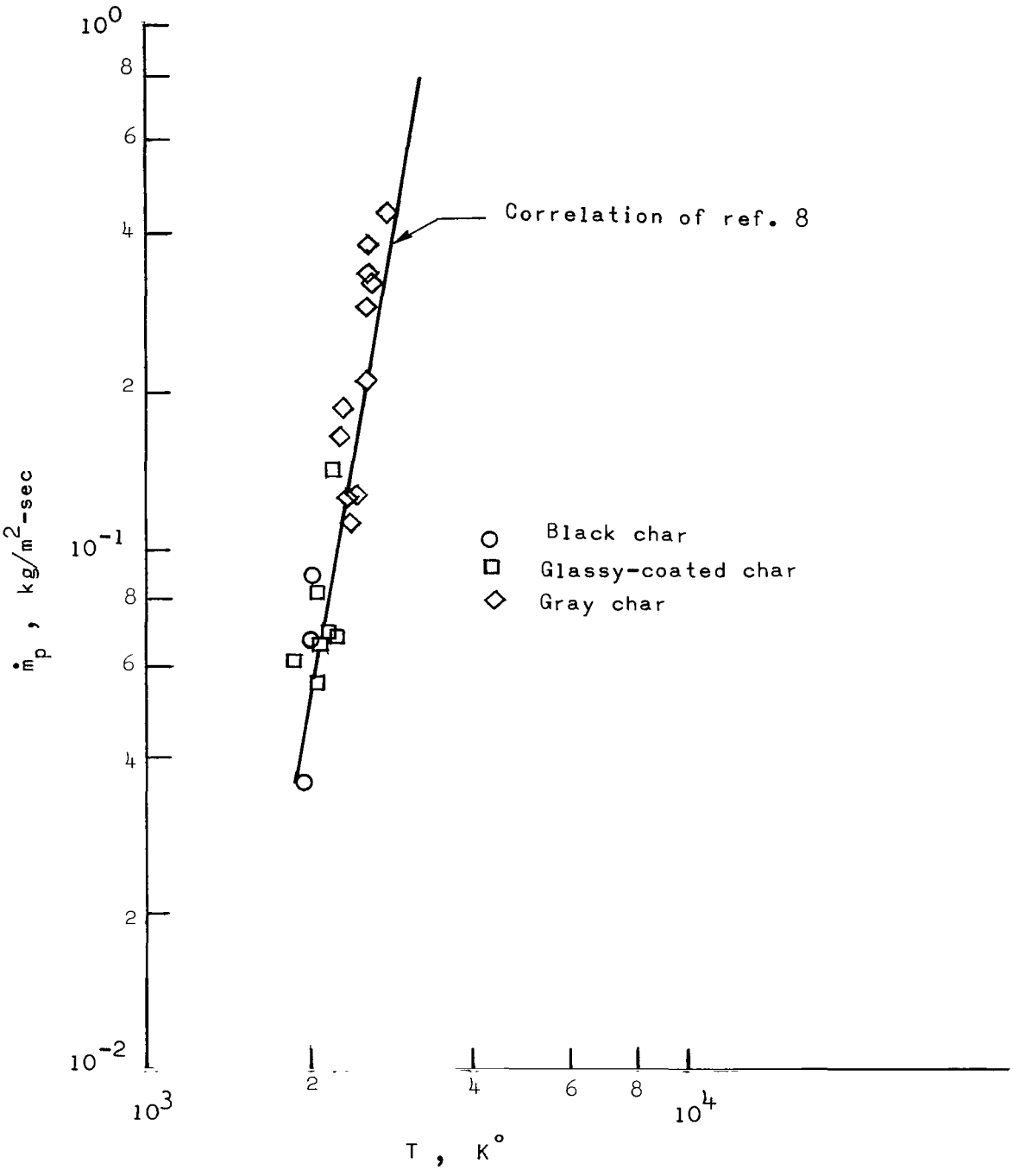

Figure 13.- Comparison between virgin-material mass loss determined in this study with the correlations of reference 8. Surface temperatures corrected with an assumed emissivity of 1.0.

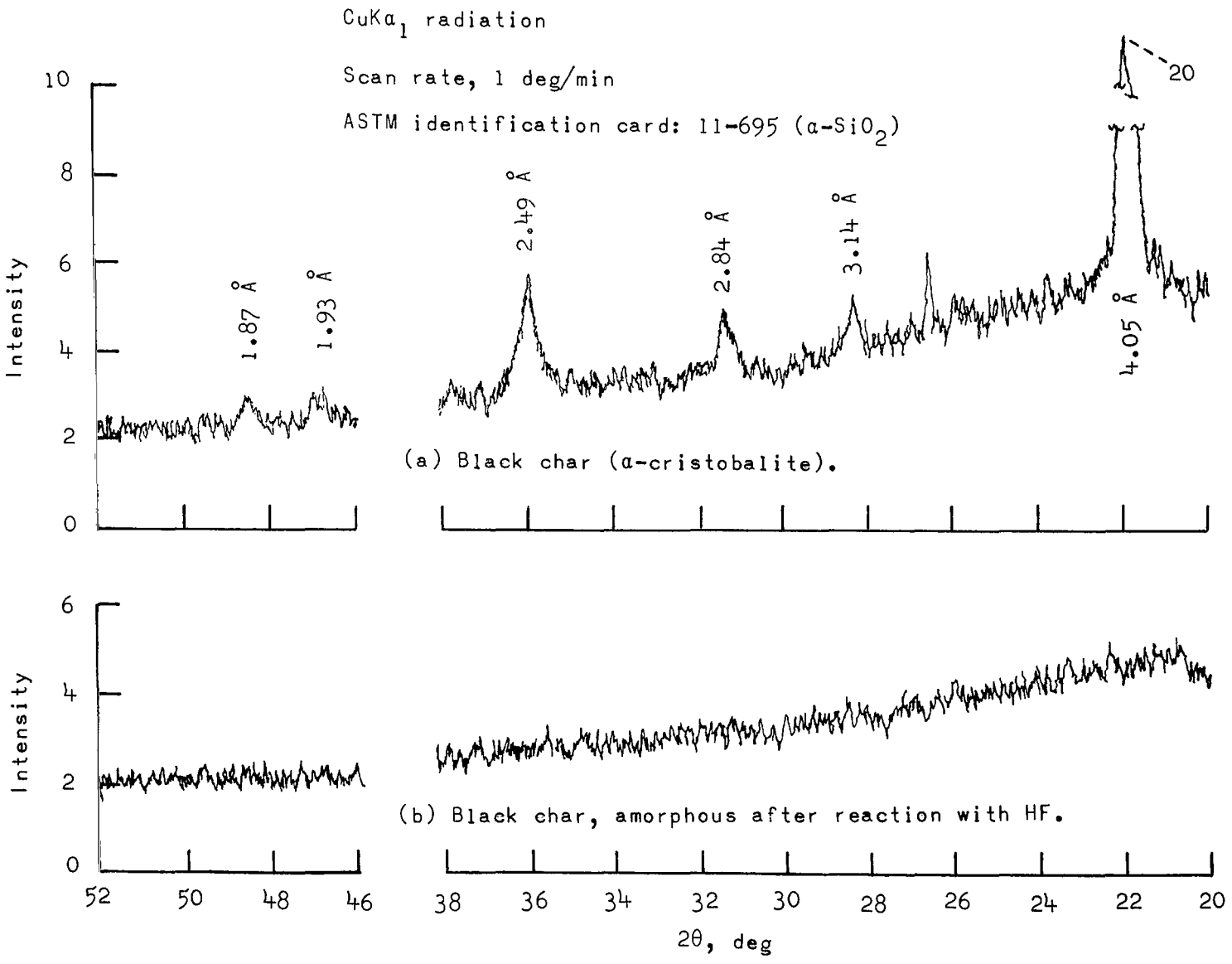

Figure 14.- Typical X-ray diffraction patterns for the black char layers before and after reactions with hydrofluoric acid.

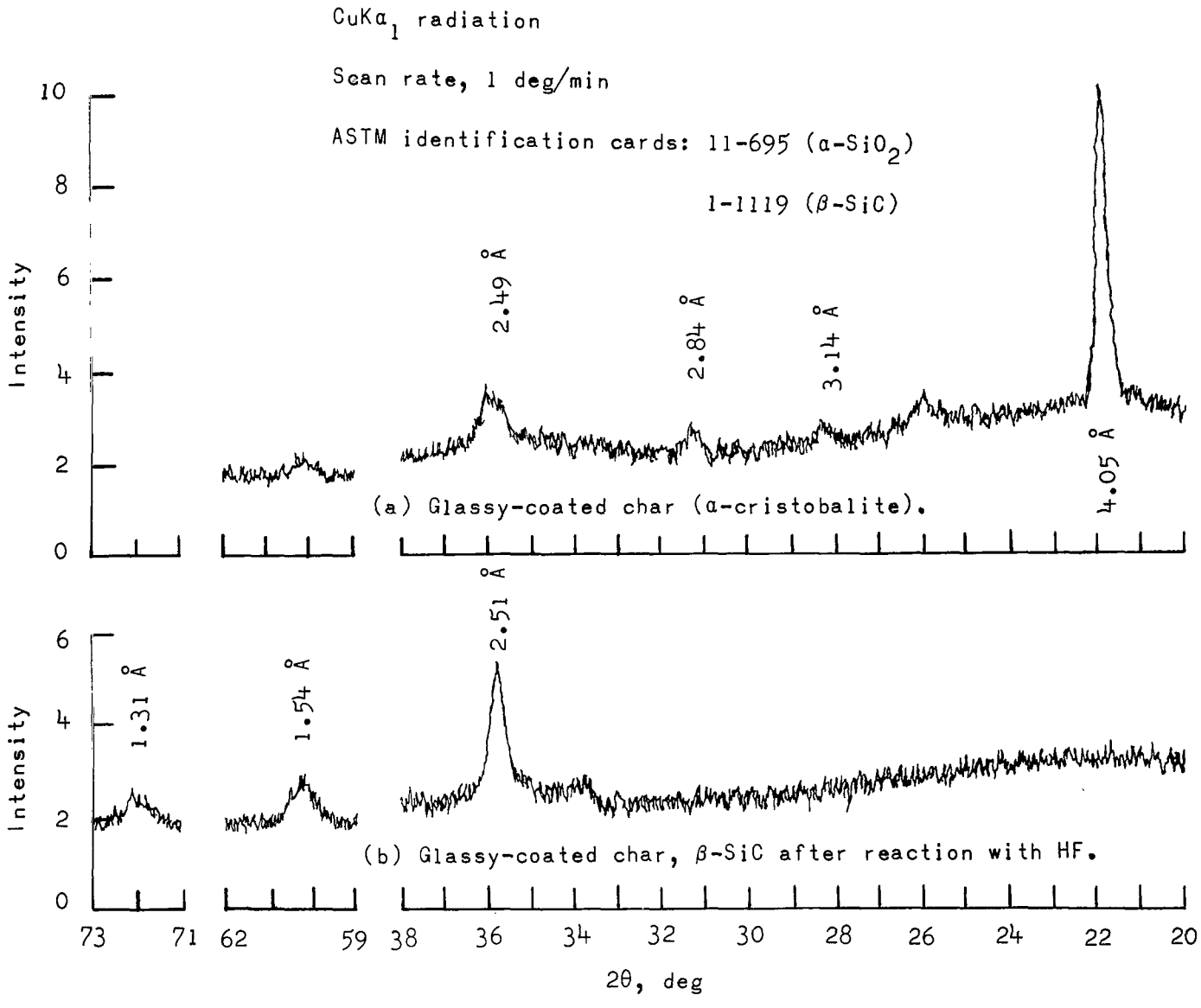

Figure 15.- Typical X-ray diffraction patterns for sublayer of glassy-coated chars before and after reaction with hydrofluoric acid.

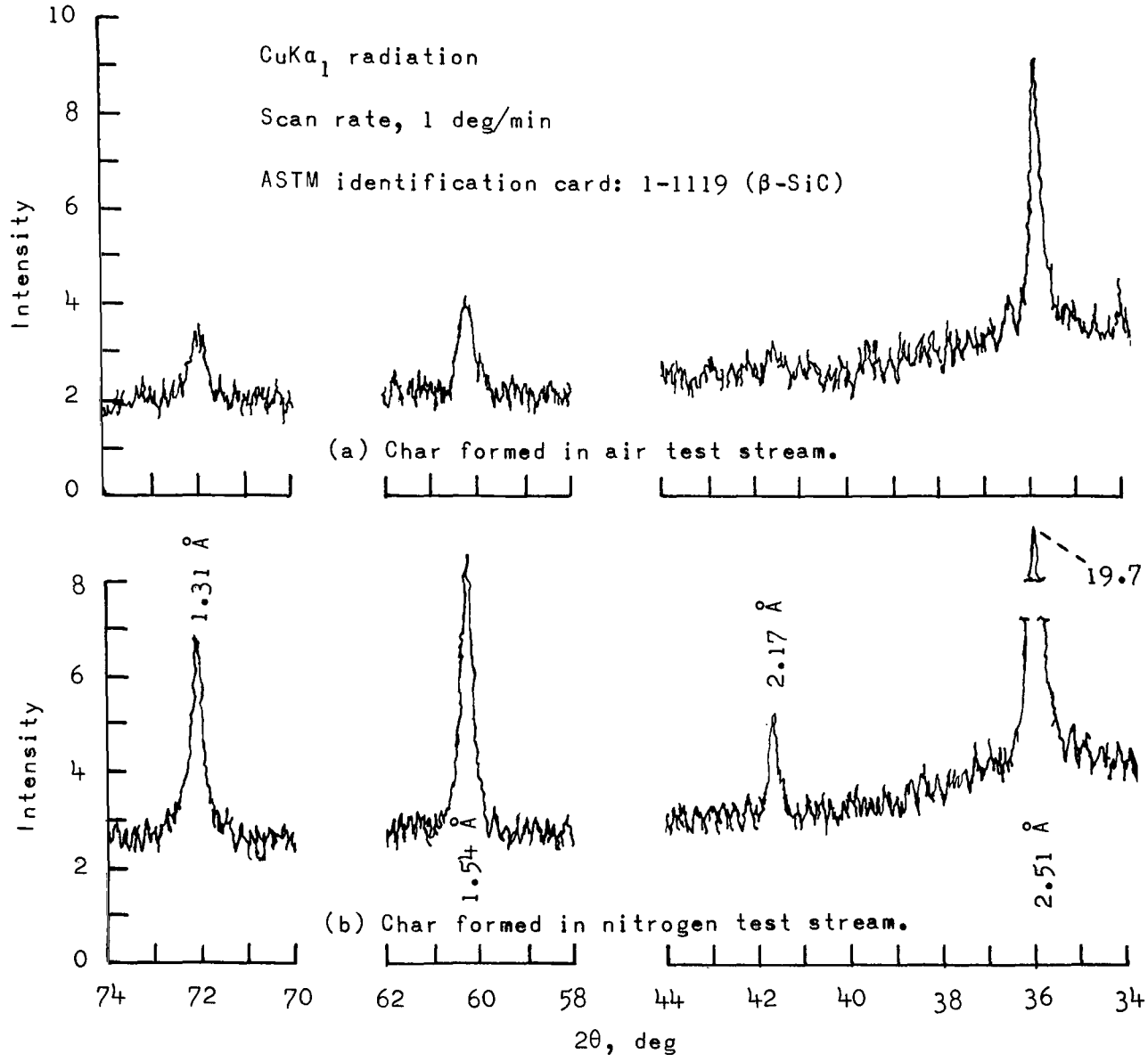

Figure 16.- Comparison of X-ray diffraction patterns for chars formed in air and pure nitrogen test streams.

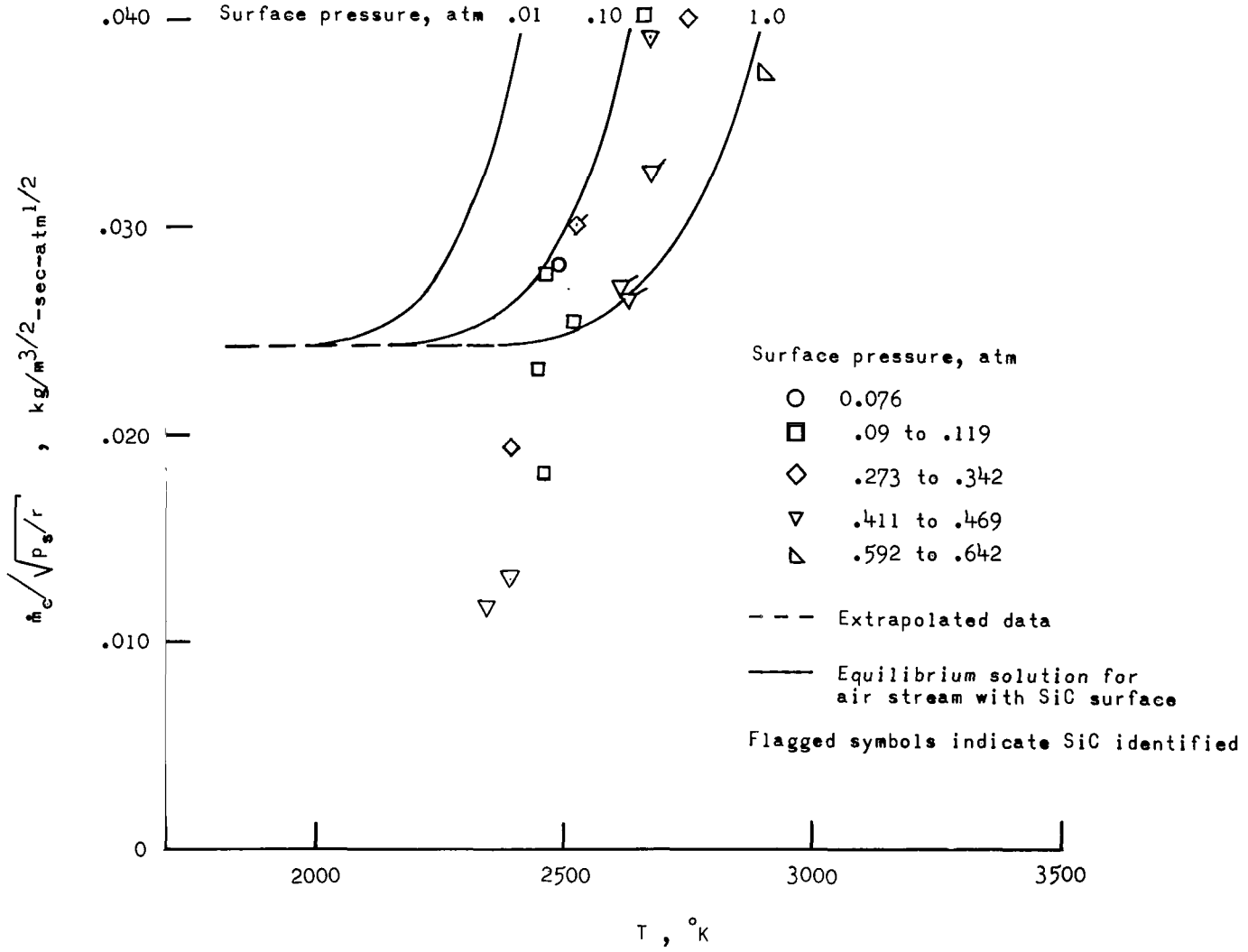

Figure 17.- Comparison of steady-state equilibrium chemical mass loss in air with experimental results. Assumptions: $\epsilon = 0.75$; $\dot{m}_g/\dot{m}_c = 2.0$.

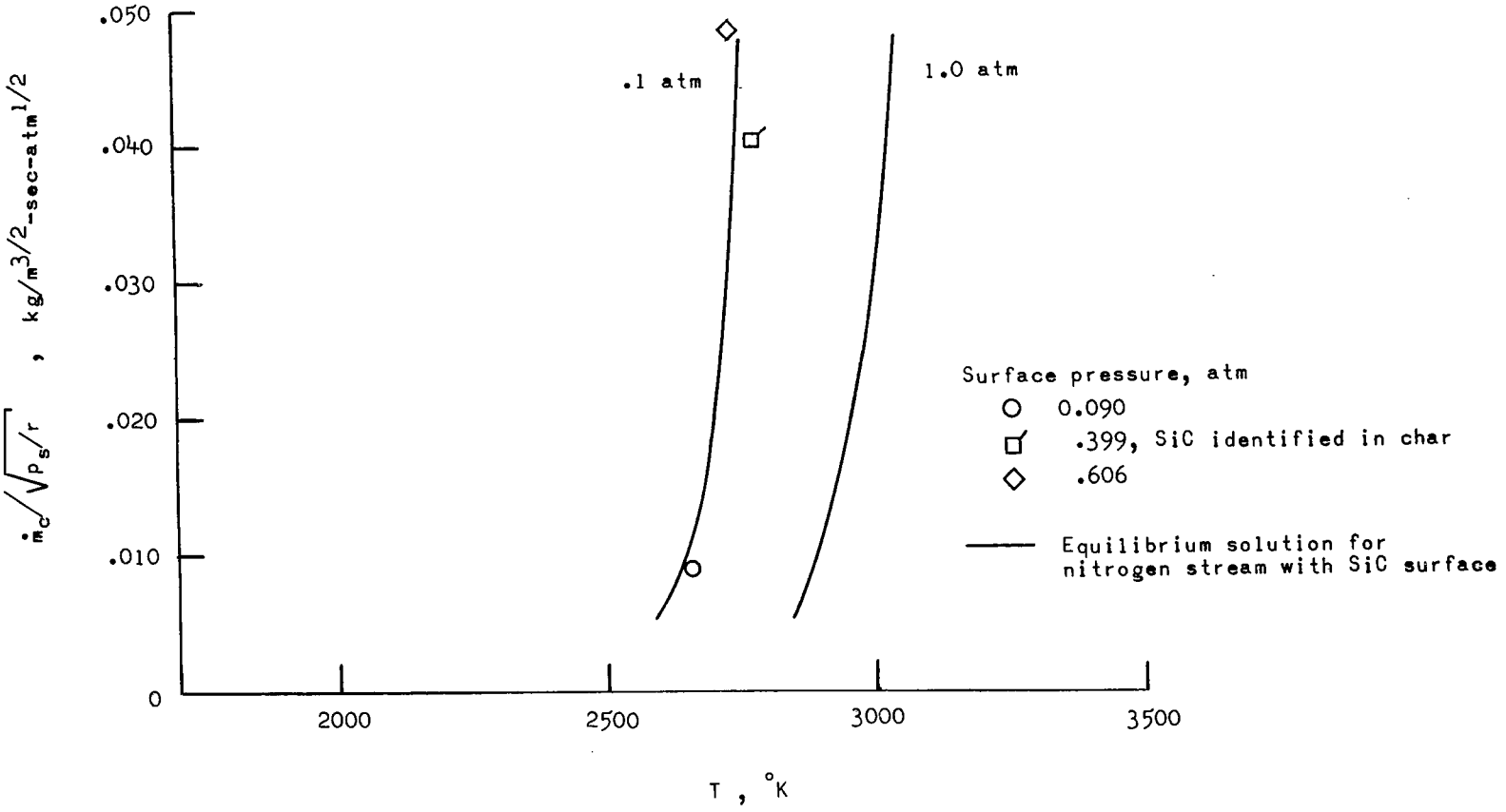

Figure 18.- Comparison of steady-state equilibrium chemical mass loss in nitrogen with experimental results. Assumptions: $\epsilon = 0.75$; $\dot{m}_g/\dot{m}_c = 2.0$.

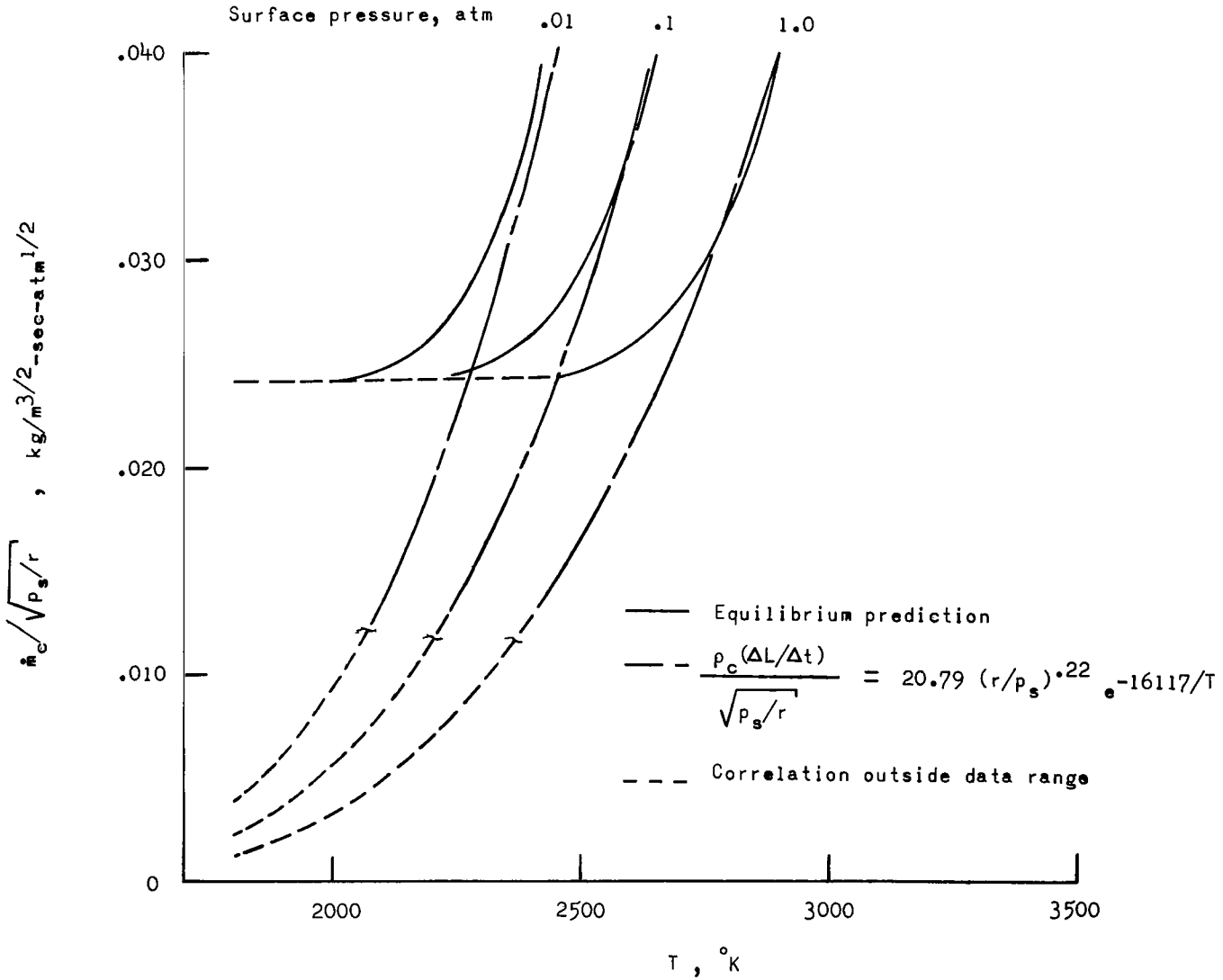

Figure 19.- Comparison of steady-state equilibrium chemical mass loss with the experimental correlation of figure 10.

"The aeronautical and space activities of the United States shall be conducted so as to contribute . . . to the expansion of human knowledge of phenomena in the atmosphere and space. The Administration shall provide for the widest practicable and appropriate dissemination of information concerning its activities and the results thereof."

—NATIONAL AERONAUTICS AND SPACE ACT OF 1958

NASA SCIENTIFIC AND TECHNICAL PUBLICATIONS

TECHNICAL REPORTS: Scientific and technical information considered important, complete, and a lasting contribution to existing knowledge.

TECHNICAL NOTES: Information less broad in scope but nevertheless of importance as a contribution to existing knowledge.

TECHNICAL MEMORANDUMS: Information receiving limited distribution because of preliminary data, security classification, or other reasons.

CONTRACTOR REPORTS: Scientific and technical information generated under a NASA contract or grant and considered an important contribution to existing knowledge.

TECHNICAL TRANSLATIONS: Information published in a foreign language considered to merit NASA distribution in English.

SPECIAL PUBLICATIONS: Information derived from or of value to NASA activities. Publications include conference proceedings, monographs, data compilations, handbooks, sourcebooks, and special bibliographies.

TECHNOLOGY UTILIZATION PUBLICATIONS: Information on technology used by NASA that may be of particular interest in commercial and other non-aerospace applications. Publications include Tech Briefs, Technology Utilization Reports and Notes, and Technology Surveys.

Details on the availability of these publications may be obtained from:

SCIENTIFIC AND TECHNICAL INFORMATION DIVISION

NATIONAL AERONAUTICS AND SPACE ADMINISTRATION

Washington, D.C. 20546